

A ROBOT MOUNTED ELECTROMAGNETIC INDUCTION SYSTEM FOR
IDENTIFICATION OF A UXO FREE CORRIDOR

Except where reference is made to the work of others, the work described in this thesis is my own or was done in collaboration with my advisory committee. This thesis does not include proprietary or classified information.

Depthi Gautam

Certificate of Approval:

Prathima Agrawal
Professor
Electrical and Computer Engineering

Lloyd S.Riggs, Chair
Professor
Electrical and Computer Engineering

Robert Dean
Assistant Professor
Electrical and Computer Engineering

George T. Flowers
Dean
Graduate School

A ROBOT MOUNTED ELECTROMAGNETIC INDUCTION SYSTEM FOR
IDENTIFICATION OF A UXO FREE CORRIDOR

Deepthi Gautam

A Thesis

Submitted to

the Graduate Faculty of

Auburn University

in Partial Fulfillment of the

Requirements for the

Degree of

Master of Science

Auburn, Alabama
December 18, 2009

A ROBOT MOUNTED ELECTROMAGNETIC INDUCTION SYSTEM FOR
IDENTIFICATION OF A UXO FREE CORRIDOR

Deepthi Gautam

Permission is granted to Auburn University to make copies of this thesis at its discretion, upon the request of individuals or institutions and at their expense. The author reserves all publication rights.

Signature of Author

Date of Graduation

THESIS ABSTRACT

A ROBOT MOUNTED ELECTROMAGNETIC INDUCTION SYSTEM FOR
IDENTIFICATION OF A UXO FREE CORRIDOR

Deepthi Gautam

Master of Science, December 18, 2009
(B.E., Osmania University, 2005)

76 Typed Pages

Directed by LLoyd S. Riggs

This thesis gives a complete overview of a time domain electromagnetic induction system developed for identification of a UXO free corridor. An EMI sensor typically consists of the transmitter and receiver coils to induct and capture the induced signal. Receiver coil amplifier circuitry is used to enhance the captured signal and data acquisition hardware and software are employed to carefully acquire and analyze the received signal to achieve an accurate understanding of the nature of the buried object. The thesis gives a detailed description of the sensor with above mentioned components and furthermore addresses GPS location tagging of the buried targets.

A pulser was used to drive a short duration current pulse through the transmitter coil which is a 35 turn AWG 10 standard wire rectangular loop. Three different receiver coil configurations were used to get a better understanding of the detection capability based on the number of receiver coil arrays. The receiver amplifier used was a precision ultra low noise operational amplifier with low DC offset. All the data was acquired in real time with National Instruments compact RIO controller and Labview FPGA programming.

In order to validate the detection capabilities of the sensor, dynamic field measurements were conducted along 5 equidistant lanes with about 35 buried ferrous and non ferrous targets. The tests were conducted at the Air Force Research Laboratory Robotics Division

in Panama city, Florida during December 2008. The set up consisted of a 4 wheeled segway robot connected to a fiberglass trailer carrying the transmitter and receiver coils. The segway was maneuvered remotely using a wireless joystick and the acquired receiver coil data along with the GPS NMEA message was communicated wirelessly to a networked PC using a 802.11 wireless router.

Four, two and one coil pair receiver configurations were used to collect the target response. Each run consisted of data collection starting on lane 1 and following in a serpentine fashion on the remaining lanes. All the targets except a deeply buried 105mm target(at 120cm) were detected by at least one coil configuration, and the sensor proved to be a reliable detection and GPS tagging device. The signals from two “identically” wound receiver coils were subtracted using a differential amplifier. This approach allows one to identify the approximate down track location of the target since a sharp null occurs when the target is located approximately between the coils. The responses from ferrous and non ferrous targets during the early time have opposite polarities during the on time of the current pulse which provides a method to easily discriminate between the two types of metal.

It was observed that objects at a depth of 120cm(3.937ft) had a low amplitude response. The observation suggests that improvement in the receiver coil amplifier and better post signal processing techniques might further improve the detection abilities with respect to deeply buried targets. Long metal bars(fiducials) were used to mark the beginning and end of every lane but unfortunately they were placed too close to the first and last targets in each lane thus somewhat compromising the data collected from the end-lane targets.

The single receiver coil configuration response was the weakest among the three configurations probably because it had to be oriented in a cross track direction to fit atop the transmitter coil. The GPS antenna was placed in the segway robot and by knowing the distance between the antenna and the center of the coils, a latitude correction could be incorporated to achieve accurate location of the coil. Subsequent research, after the December 2008 tests at AFRL, was conducted to optimize the receiver coil amplifier. This work resulted in the ability to capture the exponential decaying response of the target over 5

orders of magnitude. High dynamic range data like this is required in order to discriminate between UXO like objects and metallic clutter.

In addition to the efforts to develop and enhance the above mentioned sensor, the real time data acquisition system along with the programming involved is also described in detail in this thesis.

ACKNOWLEDGMENTS

The present work could not have been possible without the guidance and encouragement of my adviser Dr.Lloyd S.Riggs, under whose inspiration I chose this exciting field and began to work. I will always be grateful and in debt to him for inspiring me with his extraordinary patience, modesty and friendliness. I am also grateful to Dr.Robert Dean and Dr.Prathima Agrawal for agreeing to serve on my committee. I would like to thank the ERDC team from Mississippi for their great team support and Greg Davis for his patience and guidance through the software setup. I take advantage of this opportunity to thank my best friends, Rupali, Sreeja, Anuja, Manish, Bharathi and all the people including my mom, Glynn, Ellie and Jagadeesh who were successful in pushing and encouraging me to complete my degree. Thanks also goes to Dave Patrick, in the Auburn University physics department for his help and encouragement. I would like to thank Dr.Prathima Agrawal and the Wireless Engineering Research and Education Center at Auburn University for financial assistance which helped me concentrate my time and energy on my research work.

Style manual or journal used Graduate School: Guide to preparation and submission
of theses and dissertations

Computer software used Windows XP, Latex, Miktex 2.8 and TeXnicCentre

TABLE OF CONTENTS

LIST OF FIGURES		xi
1	INTRODUCTION	1
2	THEORY OF ELECTROMAGNETIC INDUCTION	3
2.1	Configuration of an EMI system	3
2.2	Types of EMI systems	3
2.3	Circuit model of an EMI system	4
2.3.1	Transmitter and object coupling	5
2.3.2	Receiver voltage - open circuit case	9
2.4	Summary	11
3	ELECTROMAGNETIC INDUCTION SYSTEM	12
3.1	Overview	12
3.2	Pulser circuit	12
3.3	Transmitter coil	16
3.4	Receiver coil arrays	16
3.5	Adjusting the Location of the Receiver Coil Pairs with Respect to the Transmitter Coil to Produce a Null Response (Balancing the Receiver Coils) . . .	19
3.6	Receiver coil amplifier	20
3.7	Data Acquisition using National Instrument's (NI's) Compact Reconfigurable input/output (cRIO) Device.	21
3.8	Measured data theoretical comparison	21
4	DATA ACQUISITION SYSTEM	25
4.1	Compact reconfigurable I/O (cRIO) system	25
4.2	Hardware and functionality	25
4.2.1	Labview FPGA module	26
4.3	Application design	28
4.3.1	FPGA vi	29
4.3.2	Time critical loop vi	30
4.3.3	Normal priority loop	30
4.3.4	TCP connection manager at the host side	31
4.3.5	Host vi	32
4.4	GPS target tracking	32

5	MEASUREMENTS AND RESULTS	34
5.1	AFRL measurements	34
5.1.1	Post processing of data	34
5.1.2	GPS correction	35
5.1.3	4 coil array results summary	36
5.1.4	2 coil array results summary	38
5.1.5	1 coil pair results summary	39
6	CONCLUSION	42
	BIBLIOGRAPHY	43
A	DATA ACQUISITION LABVIEW CODE	44
A.1	FPGA vi	44
A.2	Time critical loop vi	45
A.3	Normal priority loop vi	46
A.4	Network manager at host PC	47
A.5	Host vi	47
B	GPS CORRECTION	53
C	TARGET LIST AND REPRESENTATION	54
D	AFRL DATA PLOTS	55

LIST OF FIGURES

2.1	Basic model of an EMI system.	4
2.2	Circuit model of (a)Pulsed EMI system (b)CW EMI system	5
2.3	Switched circuit model of a pulse EMI system.	6
2.4	Normalized transmitter current vs. normalized time.	7
2.5	Normalized object current vs the ratio of shutoff time to object time constant.	9
2.6	Representative plots for (a) Transmitter Current (b)Object Current (c)Object Coupled Receiver Voltage and (d) Direct Coupled Receiver Voltage. Dotted vertical line marks the time $t=T$	10
3.1	Complete Electromagnetic Induction (EMI) System Including remotely operated Segway “robot” and fiberglass trailer carrying the transmitter and receiver coils. The basket atop the robot contains the EMI hardware (pulser to drive excitatory current into the transmitter coil, receiver coil amplifier, National Instruments cRIO control and data acquisition, 802.11 wireless router, and the Trimble GPS navigation system).	13
3.2	Transmitter Coil Driver Circuit Diagram	14
3.3	(a)Transmitter coil waveform over several periods and (b)expanded view of the current turn-off.	15
3.4	(a)Front and (b)back view of the final pulser electronic hardware.	16
3.5	Dimensions and construction details of the transmitter coil.	17
3.6	Three different receiver coil arrays used during the course of the research project: (a.) Baseline 4-coil pair array, (b.) 2-coil pair array, and (c.) Single coil pair array.	18
3.7	Construction details of the baseline 4-coil pair receiver array.	18
3.8	Transmitter coil and baseline 4-coil pair receiver array mounted on the fiberglass cart manufactured by the Air Force Research Laboratory (AFRL) in Panama City, Fl.	19

3.9	Transmitter coil and a.) two-coil pair receiver array mounted and b.) single coil pair array mounted on the fiberglass cart manufactured by the Air Force Research Laboratory (AFRL) in Panama City, FL.	20
3.10	Circuit diagram of the receiver coil amplifier.	22
3.11	Final receiver coil amplifier package	23
3.12	National Instruments compact reconfigurable input/output (cRIO) data acquisition and control unit consisting of: cRIO chassis, real time processor, digital input/output card and analogue-to-digital converter card.	23
3.13	(a)Response of a 105mm ferrous target, (b)Response of a copper loop(non ferrous)	24
3.14	Response of a loop	24
4.1	Basic components of a cRIO system, (a)Real time controller (b)Chassis with FPGA chip (c)I/O module	26
4.2	cRIO Component functionality.	27
4.3	Typical application design.	28
4.4	Flow chart of application design.	29
4.5	Sample receiver coil data.	33
5.1	Target position and robot trajectory.	35
5.2	Superimposition of static GPS map on the data plot for position tracking.	36
5.3	Sample 4 coil pair receiver coil data of lane 1.	37
5.4	Sample 2 coil pair receiver coil data of lane 1.	38
5.5	Sample 1 coil pair receiver coil data of lane 1.	40
5.6	Detection success map	41
A.1	FPGA vi	44
A.2	Time critical loop vi	45
A.3	Normal priority loop vi	49
A.4	Network manager at host PC	50

A.5 Spectrogram waterfall logic	51
A.6 Host record and display logic	52
C.1 Target list and representative targets used in AFRL tests.	54
D.1 4Coil array response run1 lane1 west to east.	55
D.2 4Coil array response run1 lane2 east to west.	55
D.3 4Coil array response run1 lane3 west to east.	56
D.4 4Coil array response run1 lane4 east to west.	56
D.5 4Coil array response run1 lane5 west to east.	57
D.6 4Coil array response run1 lane1 east to west.	57
D.7 2Coil array response, run1 lane1 west to east.	58
D.8 2Coil array response, run1 lane2 east to west.	58
D.9 2Coil array response, run1 lane3 west to east.	59
D.10 2Coil array response, run1 lane4 east to west.	59
D.11 2Coil array response, run1 lane5 west to east.	60
D.12 2Coil array response, run1 lane1 east to west.	60
D.13 1Coil response, run1 lane1 west to east.	61
D.14 1Coil response, run1 lane2 east to west.	61
D.15 1Coil response, run1 lane3 west to east.	62
D.16 1Coil response, run1 lane4 east to west.	62
D.17 1Coil response, run1 lane5 west to east.	63
D.18 1Coil response, run1 lane1 east to west.	63

CHAPTER 1
INTRODUCTION

The term unexploded ordnance or UXO refers to explosive, propellant or chemical-containing munitions that were armed, fired and remain unexploded through malfunction[1]. UXO contamination has grown for decades and now presents a serious problem in the United States. The contamination prevents civilian land use, threatens public safety and causes environmental concerns.

Most UXO in the U.S. is the result of weapons system testing and troop training activities conducted by the DOD[2]. UXO remediation focuses on efforts to clean Formerly Used Defense Sites(FUDS) and Base Realignment And Closure(BRAC) sites. The UXO cleanup problem is a very large-scale undertaking involving 10 million acres of land at some 1400 sites[1]. Estimated clean up costs being tens of billions of dollars, the application of modern technology can yield a dramatic reduction to cost.

This thesis addresses the UXO detection potential of a time domain EMI sensor. Chapter 2 discusses the theory of electromagnetic induction followed by types of EMI sensors and a mathematical discussion on time domain EMI systems. Chapter 3 gives a detailed description of the hardware involved. The pulser which is used to excite the transmitter coil is presented along with the receiver coil amplifier and the three receiver coil configurations as well as an overview on the data acquisition system. Chapter 4 describes the real time data acquisition hardware used with a flow chart provided describing the functioning of all modules. This chapter also presents the GPS and wireless features of the system. Chapter 5 gives the post processing and data analysis methods applied to the data and a detailed description of the results of each different receiver coil configuration followed by a success map which summarizes the results. All the final measurements results are provided

in APPENDIX D. Chapter 6 concludes the thesis with a brief overview of the research and suggestions for improvement to the EMI system.

In addition to the description of the sensor and detection results, the software program and logic is explained in detail in APPENDIX A along with screen shots of the code. Since the programming language used was graphical, with data flow programming techniques, all the code could not be presented, but the essential information is provided so that if necessary, new technology can be easily added to the data acquisition system.

CHAPTER 2

THEORY OF ELECTROMAGNETIC INDUCTION

This chapter gives an overview of the basic principle of electromagnetic induction[3],[4]. Types of EMI systems and an analytical representation of a time domain EMI system is presented.

2.1 Configuration of an EMI system

Figure 2.1 gives an idea of a typical EMI system model consisting of a transmitter coil, receiver coil and a buried object. The transmitter coil when excited with a time varying current, radiates a primary magnetic field in its vicinity which in accordance with Faraday's law induces an emf in the nearby buried conductive object and the receiver coil. The eddy currents in the object produce a secondary magnetic field which in turn induce a voltage in the receiver coil[5]. The receiver coil thus consists of two components of the induced voltage, one from the primary magnetic field from the transmitter coil and the other from the secondary magnetic field from the buried metallic object. Since the voltage induced by the object is of interest, the component induced by the transmitter coil is reduced using a bucking coil configuration in which each loop couples equally but oppositely thus zeroing the direct-coupled voltage component.

2.2 Types of EMI systems

Conventional EMI systems are classified into time domain and frequency domain sensors based on the type of excitation of the transmitter coil. Time domain sensors use short duration current pulses to excite the transmitter coil and are referred to as pulsed EMI systems. The current pulses are usually increased to a certain level then abruptly shut off

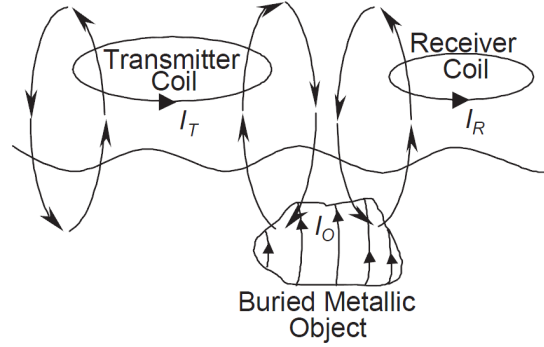


Figure 2.1: Basic model of an EMI system.

to induce an emf in the buried object. Frequency domain sensors are continuous wave (CW) EMI systems which use sinusoidal currents ranging frequency from 1 Hz to a few kilo Hz to excite the transmitter coil [6].

Both FD and TD detectors have their own advantages and limitations when it comes to metal detection and discrimination. TD detectors can operate over a higher bandwidth than FD detectors thus, high bandwidth targets are best resolved with TD detectors. In the mid bandwidth range, FD metal detectors can operate with higher power efficiency than TD metal detectors thus metal targets with mid bandwidth response are best measured with FD detectors. In the low bandwidth range, TD metal detectors can operate more efficiently compared to FD metal detectors[6].

2.3 Circuit model of an EMI system

Figure 2.2 shows the equivalent time and frequency domain circuit models of an EMI system which are basically derived from Figure 2.1. This representation is valid only for a simple first order object such as a loop of thin copper wire(radius of the wire much less than the radius of the loop) and does not hold for complex objects like cylinders and spheres. In Figure 2.2 (a) and Figure 2.2 (b), the transmitter and the receiver are represented by equivalent self inductance and resistance pairs (R, L) and subscripts T, O, R representing transmitter, object and receiver respectively. The input impedance of the receiver amplifier

being Z_R and the currents of transmitter, receiver and object being I_T, I_R, I_O respectively. Furthermore, mutual coupling between transmitter and the object, object and the receiver coil, and the transmitter and the receiver are denoted by M_{TO}, M_{OR} and M_{TR} respectively. The mutual coupling between the receiver and transmitter induces a V_{DIRECT} at the receiver coil which is undesired and may be removed by subtracting the response from identical coils as discussed earlier.

In a pulsed EMI system, which is used for the present work, it is desirable to turn off the transmitter current as rapidly as possible without any oscillations because the induced voltage in the object is proportional to the derivative of the transmitter current. A shunt resistance R_X may be used to dampen the oscillations due to the second order interaction between the parasitic capacitance and the transmitter coil inductance[7]. Similarly R_Y reduces the oscillations on the receiver side. Z_R and Z_L are the input impedances of the receiver coil amplifiers.

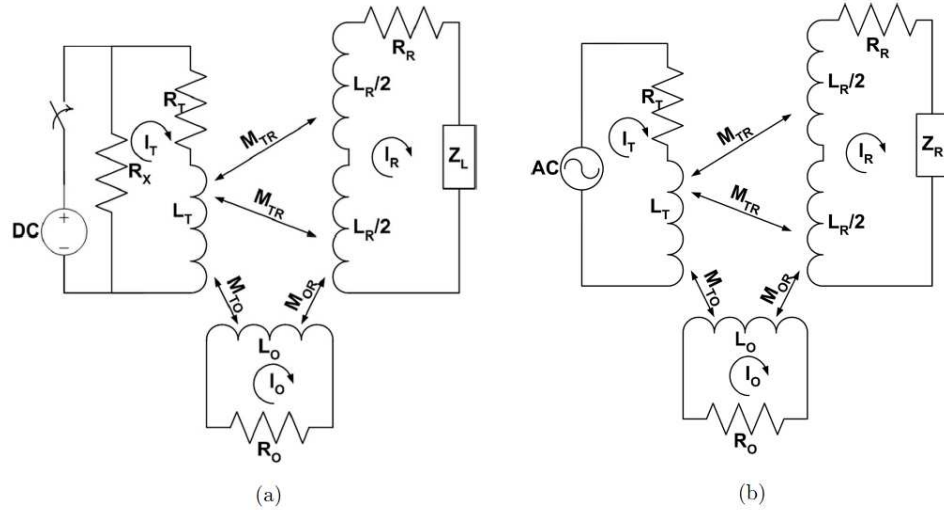


Figure 2.2: Circuit model of (a)Pulsed EMI system (b)CW EMI system

2.3.1 Transmitter and object coupling

A switched circuit model shown in figure 2.3 can be used to illustrate the time domain EMI system where the closed circuit represents the case when the transmitter is excited with

current pulses and the open circuit when they are turned off. If a current I_T flows through the transmitter then the voltage induced in the object, V_{OBJ} according to Faraday's law[8], is the product of mutual coupling between the transmitter and the object and the time rate of change of the transmitter current

$$V_{OBJ} = -M_{TO} \frac{dI_T}{dt} \quad (2.1)$$

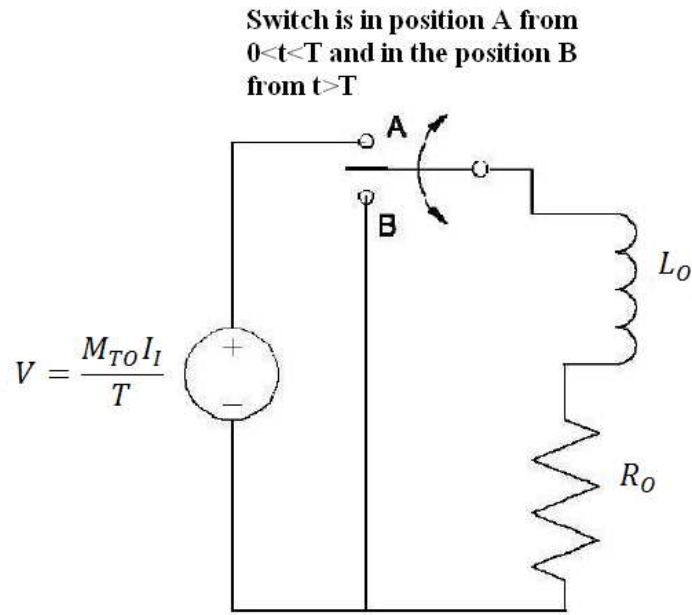


Figure 2.3: Switched circuit model of a pulse EMI system.

A transmitter current I_T which is illustrated in Figure 2.4 has an initial value I_I , for all times $t < 0$, and for times $0 < t < T$, linearly decreases until it is zero at $t = T$ as an ideal case. Since the transmitter current $I_t(t)$ for time $t < 0$, the induced voltage in the object is zero, and while the switch is in position A, the transmitter current decays linearly ($0 \leq t \leq T$), and the voltage induced in the object is constant and is equal to $\frac{M_{TO} I_I}{T}$. During this period, the eddy currents exponentially increase as shown in the Figure 2.6(b).

The object current, $I_O(t)$, when the switch is in position A can be written as,

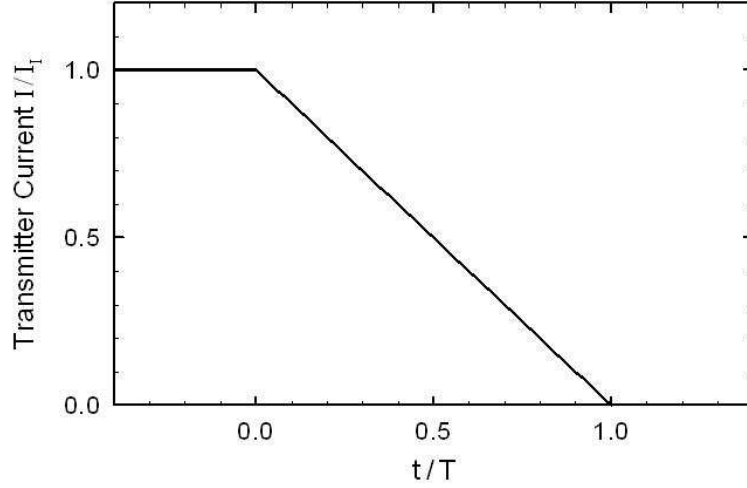


Figure 2.4: Normalized transmitter current vs. normalized time.

$$I_O(t) = K_1 + K_2 e^{-\frac{t}{\tau_0}} \quad (2.2)$$

where $\tau_0 = \frac{L_O}{R_O}$ is the time constant of the object. At time $t=0$, the object current is zero and (2.2) yields, $I_O(t=0) = k_1 + k_2$ or

$$k_1 = -k_2 \quad (2.3)$$

If the switch was left in position A indefinitely, the current would asymptotically approach V_{OBJECT}/R_O which yields to

$$I_O(t = \infty) = \frac{V_{OBJECT}}{R_O} = K_1 \quad (2.4)$$

Using (2.3) and (2.4) in (2.2) yields,

$$I_O(t) = \frac{M_{TO} T_I}{T R_O} (1 - e^{-\frac{t}{\tau_0}}) \quad (2.5)$$

which is the charge up current of the object, valid only for $0 \leq t \leq T$. The object current reaches a maximum value at time T , given by,

$$I_O(t = T) = \frac{M_{TO}I_I}{TR_O}(1 - e^{-\frac{T}{\tau_o}}) \quad (2.6)$$

At time $t=T$, the voltage induced in the object becomes zero, as the transmitter current no longer changes. Therefore, the peak current in equation (2.6), starts to decay exponentially to zero starting at $t=T$. When the switch in Figure 2.3 is in position 'B' ($T \leq t \leq \infty$), the object current is given by,

$$I_O(t = T) = \frac{M_{TO}I_I}{TR_O}(1 - e^{-\frac{T}{\tau_o}})e^{-\frac{(t-T)}{\tau_o}}u(t - T) \quad (2.7)$$

Where $u(t)$ is the unit step function. The peak object current in equation (2.6) can also be expressed as,

$$I_O\left(\frac{T}{\tau_o}\right) = \frac{M_{TO}I_I}{L_O} \frac{(1 - e^{-\frac{T}{\tau_o}})}{\frac{T}{\tau_o}} \quad (2.8)$$

If $\frac{M_{TO}I_I}{L_O}$ is taken as a constant, then the peak object current at the time $t=T$ takes the form,

$$y(x) = \frac{1 - e^{-x}}{x} \quad (2.9)$$

with $x=\frac{T}{\tau_o}$ the equation (2.9), by L'Hospital's rule, is maximum when $x=\frac{T}{\tau_o} = 0$ or when the current shutoff time is much less than the time constant of the object, $T \ll \tau_o$. Figure 2.5 shows a plot of the normalized peak current as a function of the ratio of the turnoff time to the object time constant. From figure 2.5, it is evident that the peak object current is maximum when $x=0$ or when $T \ll \tau_o$ or $\tau_o \gg T$. Therefore, the turn-off time of the transmitter current should be much less than the object time constant to maximize the object current. The concept gives a possibility that the transmitter coil current turn off time T can be adjusted to suppress the responses of small objects with fast decay rates in favor of large objects with slow decay rate[9]. This idea can be put to use if one wishes to suppress the response of clutter and decrease false alarms. And a linear turn off is superior

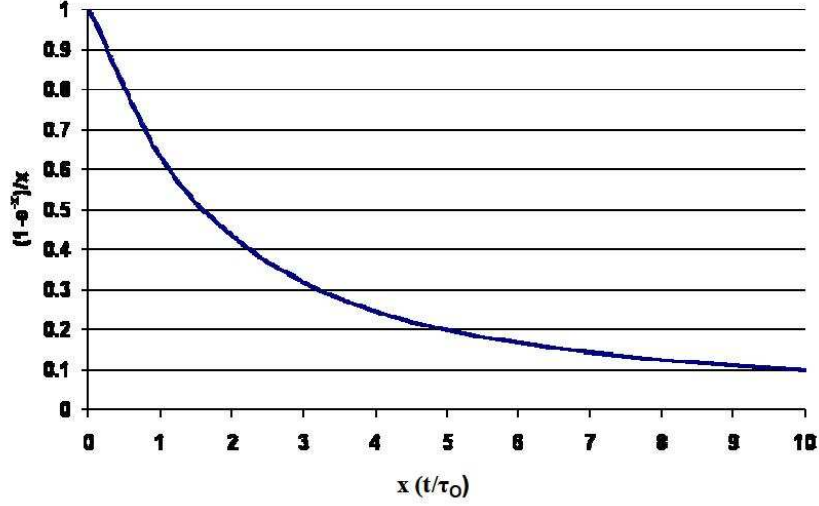


Figure 2.5: Normalized object current vs the ratio of shutoff time to object time constant.

to exponential turn off because exponential function only approaches zero after a very long time and it might delay the rebound from saturation.

2.3.2 Receiver voltage - open circuit case

The receiver coil voltage(V_{OR}) can be obtained in a similar fashion like the voltage of the object was calculated in section 2.3.1. According to Faraday's law, V_{OR} is determined by multiplying the derivative of the object current and the mutual coupling between the object and the receiver coil,

$$V_{OR} = M_{OR} \frac{dI_O(t)}{dt} \quad (2.10)$$

If $T/\tau_o \ll 1$, then a Taylor series expansion of (2.5) provides a linear approximation, $\widetilde{I}_o(t) = \frac{M_{TO}I_I}{T L_O} t$ for the object current during the time $0 \leq t \leq T$, which is shown in Figure 2.6(b) as the dashed line. Substituting $\widetilde{I}_o(t)$ in (2.10) gives,

$$V_{OR}(t) = \frac{M_{OR}M_{TO}I_I}{L_O T}, 0 \leq t \leq T \quad (2.11)$$

Similarly substituting (2.7) in (2.10) for $t \geq T$ gives

$$V_{OR}(t) = -\frac{M_{OR}M_{TO}I_I}{\tau_o T R_o} (1 - e^{-\frac{T}{\tau_o}}) e^{-\frac{(t-T)}{\tau_o}}, t \geq T \quad (2.12)$$

Using a Taylor series expansion in (2.12), the voltage induced in the receiver coil for $t \geq T$ can be written as

$$V_{OR}(t) = -\frac{M_{OR}M_{TO}I_I}{\tau_o T R_o} e^{t/\tau_o}, t \geq T \quad (2.13)$$

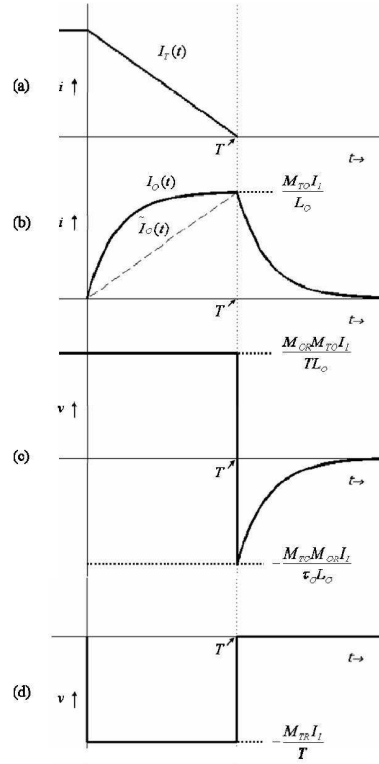


Figure 2.6: Representative plots for (a) Transmitter Current (b) Object Current (c) Object Coupled Receiver Voltage and (d) Direct Coupled Receiver Voltage. Dotted vertical line marks the time $t=T$.

Since the ratio of voltages in (2.11) and (2.13), is τ_o/T and since $\tau_o/T \gg 1$, the receiver voltage drops rapidly from the maximum value to the lower limit at $t=T$, and then the exponential decay starts, as shown in Figure 2.6(c). There is also a direct coupled component at the receiver due to coupling between the transmitter and the receiver which can be represented as

$$V_{DIRECT} = -M_{TR} \frac{d}{dt} I_T(t) = \begin{cases} 0 & t < 0 \\ \frac{M_{TRL}}{T} & 0 \leq t \leq T \\ 0 & t > T \end{cases} \quad (2.14)$$

The direct coupled receiver voltage is shown in Figure 2.6(d) And as mentioned earlier, with appropriate design, the direct coupling between the transmitter and receiver is greatly reduced and the residual coupling can be denoted as M_{TR}^r (superscript r represents residual) then

$$V_{\infty}^r(t) = \pm M_{TR}^r \frac{dI_T(t)}{dt} \quad (2.15)$$

The sign of the direct coupled voltage depends upon the winding direction of the halves of the receiver coil with respect to that of the transmitter coil and upon which half has the larger direct coupling. Therefore it is possible for the direct-coupled voltage to either add or subtract from the object coupled receiver voltage for times $0 \leq t \leq T$

2.4 Summary

This chapter presented the basic concepts of an EMI sensor followed by a circuit analysis to describe the characteristics of a time domain EMI system. The design and development of a pulsed EMI sensor setup with the data acquisition hardware will be discussed next with experimental results presented in the following chapters.

CHAPTER 3
ELECTROMAGNETIC INDUCTION SYSTEM

3.1 Overview

In this section a description of the EMI system is provided. As shown in Figure 3.1, the system consists of a 4-wheeled remotely controlled Segway "robot" connected to a two-wheeled trailer that carries the EMI coils (transmitter and receiver). The EMI coils radiate and receive low frequency magnetic fields that are used to detect the presence of buried metallic objects (UXO). The basket atop the Segway robot contains the EMI electronic hardware components as well as the GPS positioning equipment. In particular, the basket contains a 12 volt utility tractor battery that powers all the on board electronic equipment. Additionally, there is an 802.11 wireless router that allows sensor data to be transferred back to the user and a separate 802.11 wireless router used to send guidance commands to the robot. The basket also contains circuitry designed to drive a short duration current pulse through the transmitter coil. (This device, shall hereafter be referred to as the pulser, and will be described in greater detail subsequently.) In addition to the items described above, the basket contains the receiver coil pre-amplifier and the National Instruments data acquisition and control electronics. The components of the EMI system are described in detail further below.

3.2 Pulser circuit

The purpose of the pulser is to drive a short duration current pulse through the transmitter coil. In order for the EMI system to have good sensitivity, the pulse should rise up to some relatively high value of current (around 10 to 15 amps) and then "turn off" relatively quickly, and most importantly, without oscillation. Two design approaches were pursued



Figure 3.1: Complete Electromagnetic Induction (EMI) System Including remotely operated Segway “robot” and fiberglass trailer carrying the transmitter and receiver coils. The basket atop the robot contains the EMI hardware (pulser to drive excitatory current into the transmitter coil, receiver coil amplifier, National Instruments cRIO control and data acquisition, 802.11 wireless router, and the Trimble GPS navigation system).

during the development of the pulser. The first centered around the power operational amplifier PA50 sold by APEX micro technology. Although this design approach showed promise, and had several very desirable features, it was eventually abandoned in favor of a simpler alternative. The final design approach was based on a simple MOSFET switch.

As shown in Figure 3.2, the circuit schematic for the pulser consists of an inductance L with series resistance R representing the electrical parameters of the transmitter coil. In parallel with the coil is four zener diodes, a capacitor, and another resistance R_s . The capacitor represents the parasitic capacitance of the transmitter coil. The MOSFET switch is connected between the coil and ground and the gate of the MOSFET is driven by a MOSFET Driver that is in turn fed by a TTL pulse train circuit. When the TTL pulse goes high (+ 5 volts) the MOSFET driver circuit also goes high, but to the full power supply voltage, +12 volts. The Mosfet driver also has the ability to sink several amps of current and can therefore quickly charge the MOSFET gate capacitance and thereby completely turn the MOSFET on (force the MOSFET into saturation). When the MOSFET turns completely on (switch closed) the current in the transmitting coil begins to increase exponentially

towards a final value of current determined by the power supply voltage (12 volts) divided the coil resistance plus the on resistance of the MOSFET. (The sum of the coil resistance and MOSFET on resistance is only a fraction of an Ohm). Once the current through the transmitting coil increases to near its final value (for our design around 15 amps) the TTL pulse turns off (0 volts) turning the MOSFET Driver off and so the MOSFET switch opens (limiting current flow).

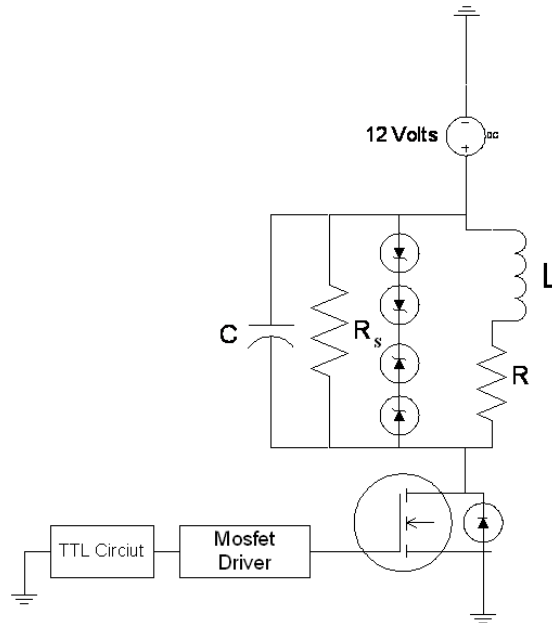
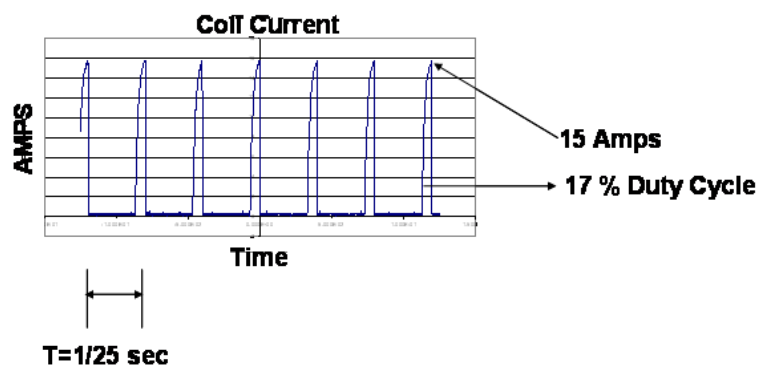


Figure 3.2: Transmitter Coil Driver Circuit Diagram

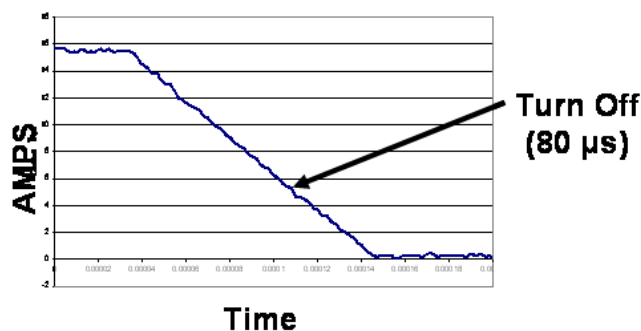
As mentioned briefly above, it is important to carefully control how the current is extinguished. When the current turns off there is a relatively large back emf (voltage) induced in the coil. (According to Faraday's law the back emf is equal to the inductance of the coil, L , times the time rate of change of the current ($v=L\frac{di}{dt}$). Zener diodes force the voltage across the coil to remain constant and therefore, once again according to Faraday's law, the current must decay ("turn off") linearly. As mentioned above the capacitance C in the circuit represents parasitic coil capacitance and so some "ringing" (oscillatory behavior, at a frequency given by $\frac{1}{2\pi\sqrt{LC}}$) of the current is expected. The shunt resistance R is

adjusted to eliminate this ringing. The shunt value of resistance is large (several hundred Ohms) in comparison to the resistance of the coil.

Figure 3.3a shows the current pulse train delivered by the pulser. Current pulses flowing through the transmitter coil repeat every 1/25th second (every 40 milliseconds). As described above the current pulses exponentially increase to around 15 amps and then, as shown in Figure 3.3(b), linearly decrease to zero in around 80 microseconds. The current pulses have a 17% duty cycle (on time of 6.8 milliseconds) and so the current remains "off" for 33.2 milliseconds between pulses.



(a)



(b)

Figure 3.3: (a) Transmitter coil waveform over several periods and (b) expanded view of the current turn-off.

Figures 3.4a and 3.4b show the physical construction of the pulser. The smaller switch, when in the on position, applies the amplified TTL pulse train to the MOSFET gate whereas

the larger switch connects the 12 volt battery to the circuit. (Both switches must be in the on position for the pulser to operate.) Two wires from the pulser connect to the 12 volt battery, and two to the transmitting coil. The smaller pair of wires connect the TTL pulse to the MOSFET driver.

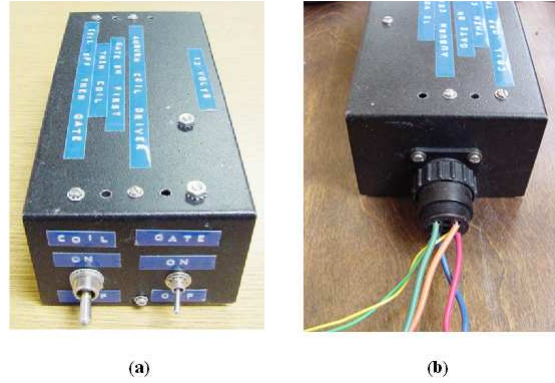


Figure 3.4: (a)Front and (b)back view of the final pulser electronic hardware.

3.3 Transmitter coil

As shown in Figure 3.5, the transmitting coil frame is 140 cm X 80 cm and is surrounded by a 5 cm deep trough which holds the coil windings. The coil consists of 35 turns of AWG 10 stranded wire with an inductance of 2.66mH and a resistance of 657m ohms. As indicated in the photograph in Figure 3.5, the coil windings are potted with spray foam to reduce vibrations. (Even small coil vibrations can result in a signal much larger than that received from a buried metallic object!) The weight of the transmitter coil frame and windings is 45.4 lbs.

3.4 Receiver coil arrays

Figure 3.6 shows the three different coil arrays that were tested during the course of this research. The left most array in the figure consists of eight individual coils that are combined in pairs to produce what will hereafter be referred to as the baseline 4-coil pair array. Similarly, the middle and rightmost figures show the two- and one-coil pair arrays.

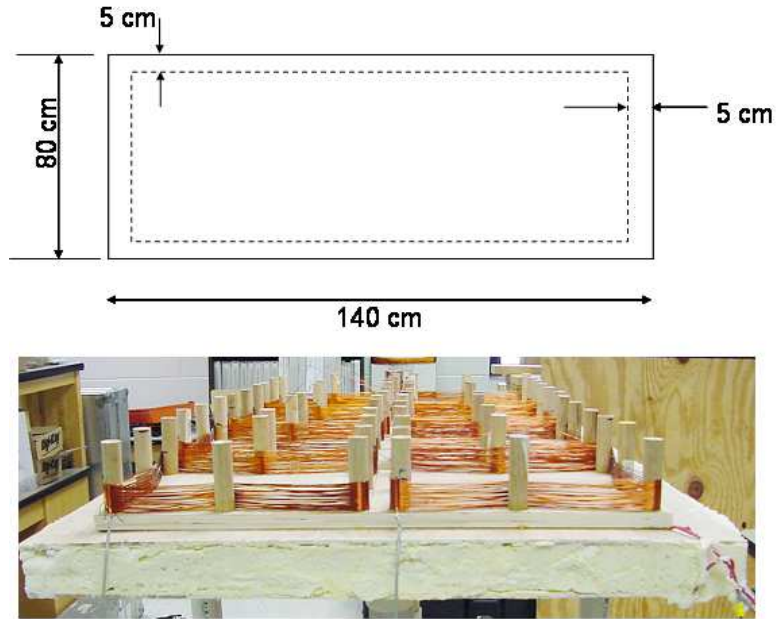


Figure 3.5: Dimensions and construction details of the transmitter coil.

Signals from coils A and B (leftmost figure) are subtracted by feeding their output into a differential amplifier. Coil pairs *C&D*, *E&F*, *G&H*, *I&J*, *K&L*, and *M&N* are similarly combined (subtracted). A metallic target located under coil A will produce a signal with positive polarity while the same target located under coil B will produce a signal with negative polarity. If a target is positioned between the two coils no signal will be produced (since each coil receives the same signal and the two are subtracted). As the array is moved down track the signal, as observed on the computer screen, will first deflect in one direction and then in the other direction with a null (no signal) in between. Because of this phenomenon the approximate down track location of the target can be easily identified. Furthermore, the cross track position of the target can be approximated by comparing the signal amplitudes from the different coil pairs. Note that the arrangement of the MN coil pair (rightmost figure) is probably not optimal since a target passing between the M and N coil will go undetected. Note finally that the down track direction is to the right in Figure 3.6.

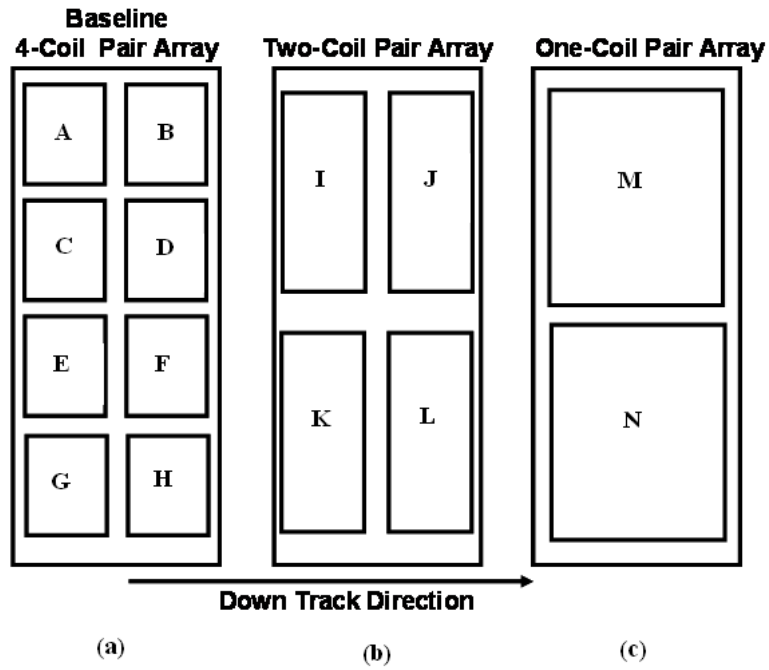


Figure 3.6: Three different receiver coil arrays used during the course of the research project: (a.) Baseline 4-coil pair array, (b.) 2-coil pair array, and (c.) Single coil pair array.

Figure 3.7 shows details of the construction of the baseline 4-coil pair array. Wooden dowels were glued into holes drilled into a sheet of 5/8 inch thick oak plywood. Next, 32 turns of 26 AWG copper enameled wire was woven around the dowels, as shown, to produce the eight individual coils.

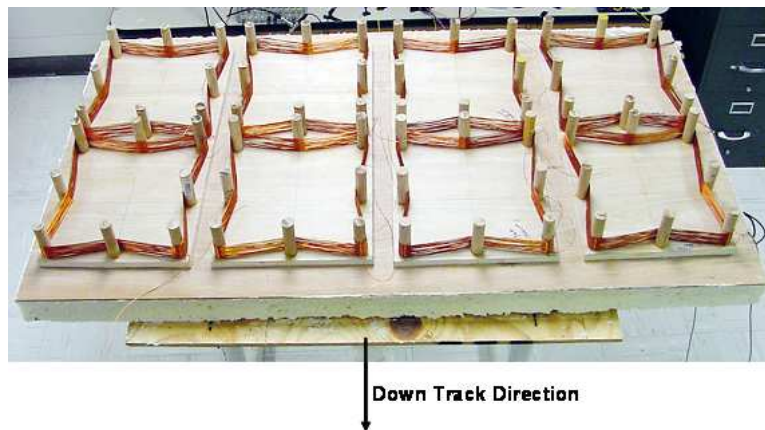


Figure 3.7: Construction details of the baseline 4-coil pair receiver array.

Figure 3.8 shows the baseline 4-coil array mounted on the fiberglass trailer that was designed and built by the Air Force Research Lab in Panama City, FL. Note that just as in the case of the transmitting coil, spray foam was used to reduce any possible vibration of the receiver coils. Note further that each coil pair is attached to the transmitter coil with fiberglass bolts. One can also observe the red and blue twisted pair wires leading to the transmitter coil and the eight BNC cables — one each connected to the receiving coils.

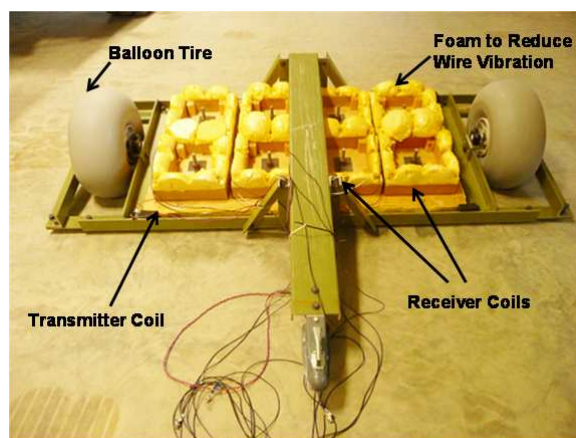


Figure 3.8: Transmitter coil and baseline 4-coil pair receiver array mounted on the fiberglass cart manufactured by the Air Force Research Laboratory (AFRL) in Panama City, FL.

3.5 Adjusting the Location of the Receiver Coil Pairs with Respect to the Transmitter Coil to Produce a Null Response (Balancing the Receiver Coils)

In the absence of any metallic target, each receiver coil pair must be symmetrically located with respect to the transmitter coil in order to produce a “null” signal. General operating procedure is to energize the EMI system and then observe the signal from each coil (as displayed on the laptop). Next, the position of the coil pair is adjusted until a null signal is observed. Once a null is obtained the fiberglass bolts are drawn down tight to eliminate movement between the transmitter and receiver coils. Figure 3.9 displays the two- and one-coil pair arrays. No effort was expended to use spray foam to secure these

coils, but they were adjusted in the manner just described to insure a null response in the absence of any metallic targets.

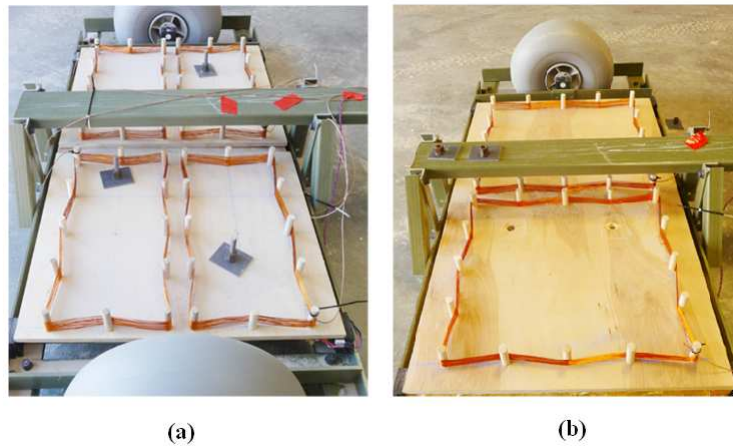


Figure 3.9: Transmitter coil and a.) two-coil pair receiver array mounted and b.) single coil pair array mounted on the fiberglass cart manufactured by the Air Force Research Laboratory (AFRL) in Panama City, FL.

3.6 Receiver coil amplifier

Weak signals from each coil pair must be amplified before being passed to the analogue-to-digital converter for further processing and display. Figure 3.10 shows the circuit diagram of the receiver coil amplifier and Figure 3.11 displays the physical construction of the amp. Linear Technology's LT1028 precision ultra low noise operational amplifier was used in the design [10]. The first two stages of the amplifier result in a voltage gain of approximately 34,000. The LT1028 has low DC offset and low DC offset drift but our design includes a potentiometer at each op-amp stage to adjust the DC offset to near zero. Note that the design also includes diode protection at the input stage. Diodes D14 through D17 insure that the input voltage does not exceed the power supply rails (plus and minus 12 volts) and damage the amplifier. The last stage of the three op-amp design serves as a simple buffer amplifier.

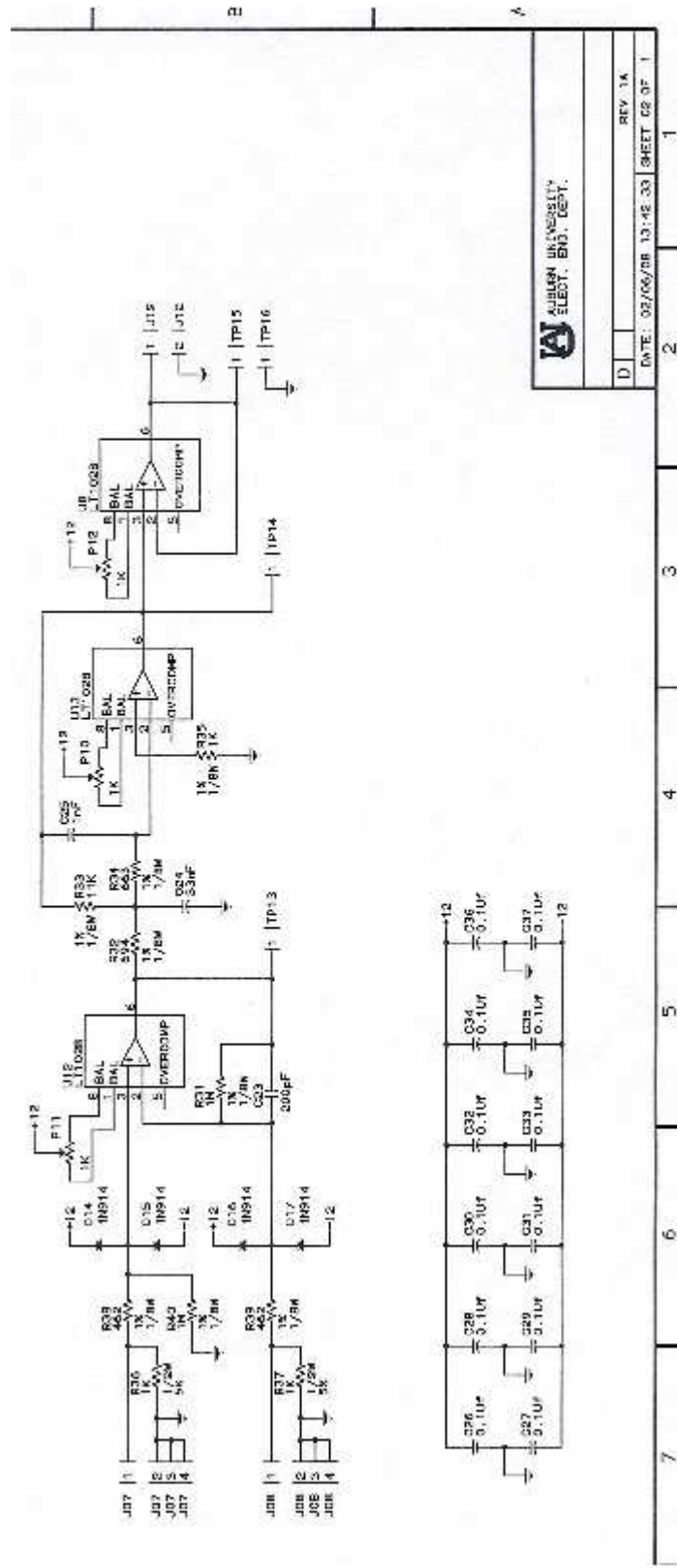
3.7 Data Acquisition using National Instrument's (NI's) Compact Reconfigurable input/output (cRIO) Device.


Figure 3.12 displays the cRIO which functions as the “brain” of our pulsed EMI system. As shown in Figure 3.12, the system consists of (1)the cRIO real time Pentium class processor (2) the chassis with 3-million gate field programmable gate array (FPGA), (3) the NI 9401 digital I/O card, and (4) the NI 9239 4-channel A/D card. The real time processor is programmed using a laptop via the ethernet port on the controller. The serial port on the controller is used to communicate with the Trimble GPS system and record, in real time, the position of the sensor. The TTL pulse that drives the pulser (see section 3.2) is generated by the NI9401 and the NI 9239 digitizes the amplified data streams coming from each receiver coil. The NI 9239 is a 24-bit A/D card with a maximum sample rate of 50 ks/sec (data point every 20 microseconds). A much more complete discussion of the cRIO is provided in the next chapter.

3.8 Measured data theoretical comparison

The above described sensor was used to collect an induction response from a copper loop(non ferrous) and a 105mm target(ferrous). Figure 3.13 gives the comparison plots of both responses and it can be seen that the response of the copper loop is opposite to the response of the ferrous object in the early time of the object response. This differentiation gives the sensor an ability to distinguish between ferrous and non ferrous objects.

Figure 3.14 gives the receiver response of a copper loop in a semi log plot. It can be observed that the decay rate is linear up to 5 orders of magnitude, which proves the dynamic range of the sensor and validates its ability as a discrimination device apart from being a good detection device.



 ALABAMA UNIVERSITY
 ELECT. ENGR. DEPT.

D	DATE: 02/06/08 13:42:33	SHEET 02 OF 1
	REV. 1A	1

Figure 3.10: Circuit diagram of the receiver coil amplifier.

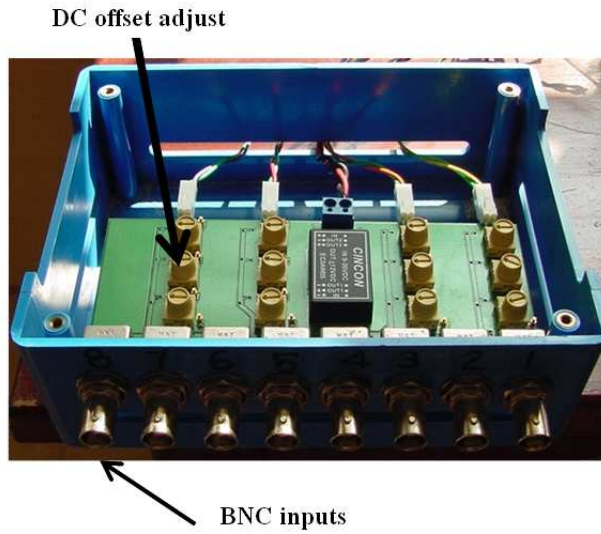


Figure 3.11: Final receiver coil amplifier package

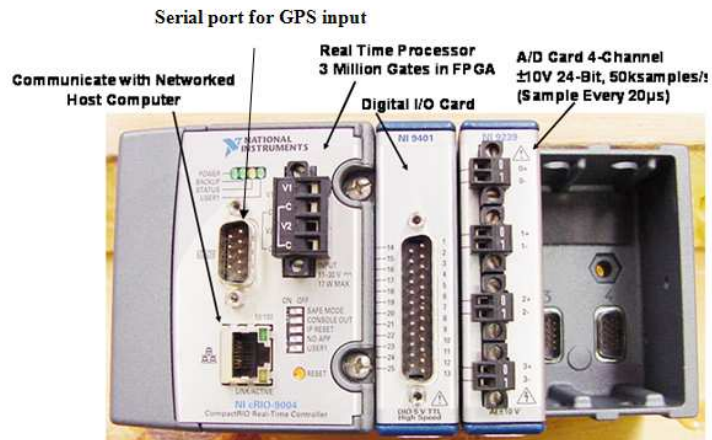


Figure 3.12: National Instruments compact reconfigurable input/output (cRIO) data acquisition and control unit consisting of: cRIO chassis, real time processor, digital input/output card and analogue-to-digital converter card.

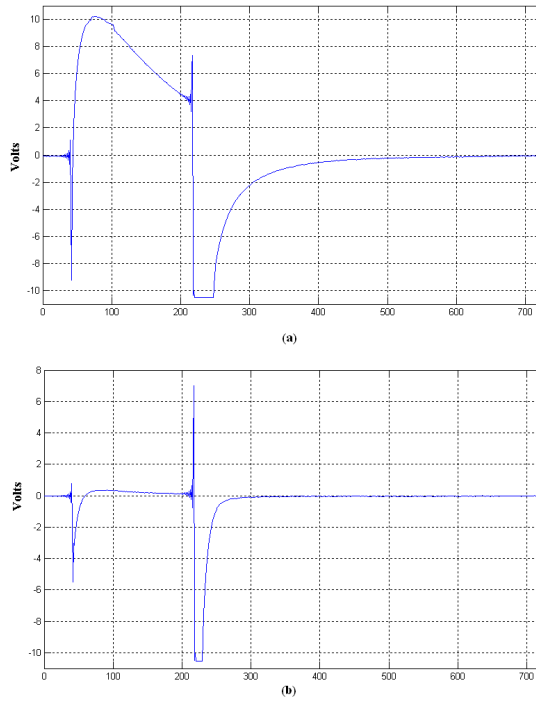


Figure 3.13: (a)Response of a 105mm ferrous target, (b)Response of a copper loop(non ferrous)

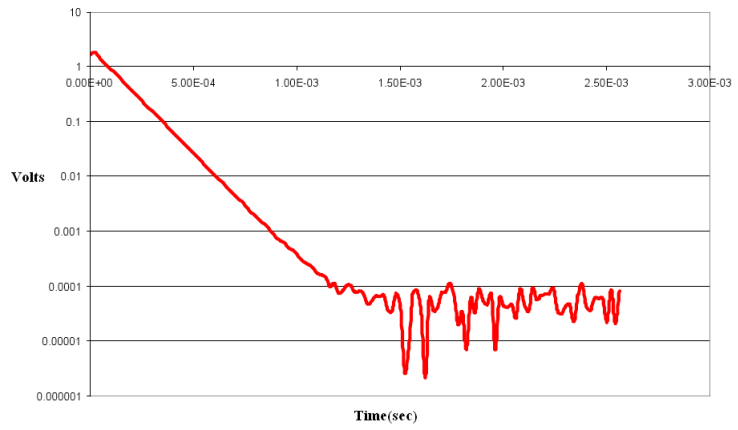


Figure 3.14: Response of a loop

CHAPTER 4
DATA ACQUISITION SYSTEM

The present chapter gives a detailed description of the data acquisition system, used for triggering, data logging and real time analysis. A general compact reconfigurable I/O (cRIO) is discussed in detail followed by the framework and flowchart of the application design. The GPS and 802.11 wireless features are also described which tag the exact locations of the targets identified followed by some field test results. The chapter concludes with the signal processing description with results presented in the next chapter.

4.1 Compact reconfigurable I/O (cRIO) system

Compact RIO by National Instruments was chosen for the present application for its small and rugged features powered by reconfigurable I/O FPGA technology. The RIO core has built-in data transfer mechanisms to pass data to the embedded processor for real-time analysis, post processing and data logging. It has the ability to communicate with a networked host computer and provide direct hardware access to the input/output circuitry of each I/O module using LabVIEW FPGA elemental I/O functions.

Figure 4.1 and Figure 4.2 give a basic idea of the components of the cRIO and their respective functionalities.

4.2 Hardware and functionality

A typical crio with the functionality described in figure 4.2 consisted of NI 9014 controller with NI 9014 8 slot chassis. The controller used has a Pentium class processor with 3 million gates in the FPGA chip embedded in the chassis with ethernet,serial,USB and SMB connector ports for data transfer and communication. The NI 9014 used for

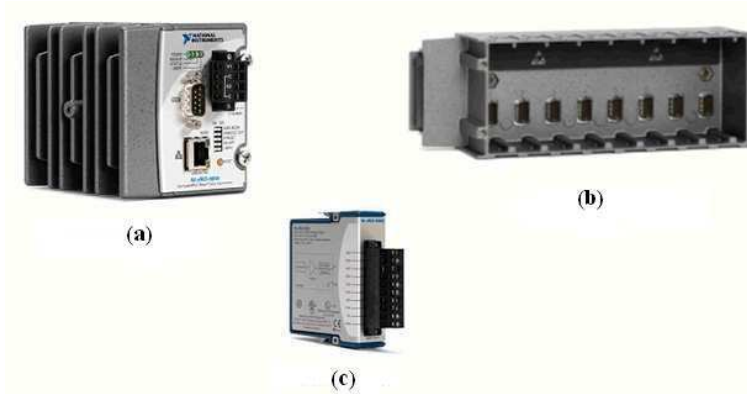


Figure 4.1: Basic components of a cRIO system, (a)Real time controller (b)Chassis with FPGA chip (c)I/O module

triggering is a 8 channel 5V/ TTL high speed bidirectional digital input/output module. The receiver data was collected using a NI 9239 which is a 4 channel 24 bit analog input module with simultaneous(each channel with the specified sampling rate) sampling rate of 50ksamples/sec.

With NI RIO technology, custom measurement hardware circuitry can be defined using reconfigurable FPGA chips and LabVIEW graphical development tools. Advantage of reconfigurable FPGA technology can be taken to automatically synthesize a highly optimized electrical circuit implementation of the input/output, communication, or control application. FPGA devices feature a reconfigurable digital architecture with a matrix of configurable-logic blocks (CLBs) surrounded by a periphery of I/O blocks. Signals can be routed within the FPGA matrix in any arbitrary manner by programmable interconnect switches and wire routes. CompactRIO offers 4 and 8-slot chassis with options for either 1 million or 3 million gate FPGA chips.

4.2.1 Labview FPGA module

Labview and the Labview FPGA Module deliver graphical development for FPGA chips on RIO hardware. With the Labview FPGA module,FPGA applications are developed on

Component	Specifications	Functionality
Real-Time processor	<ul style="list-style-type: none"> • 200MHz Pentium class processor • 11-30 VDC supply input • LED status indicators • SMB connector to use a GPS device for system clock drift correction • 10/100 Mb/s Ethernet port with built in HTTP, FTP and SMTP servers • USB support for additional storage and peripherals 	<p>Processor deterministically executes the LabVIEW Real-time application.</p> <p>Responsible for real time analysis, post processing, data logging or communication to a networked host computer</p>
Reconfigurable chassis	<ul style="list-style-type: none"> • Contains FPGA chip connected to I/O modules in star topology for precise timing and synchronization • PCI bus connection interface between the FPGA chip and the real time processor • 40MHz on board clock 	Provides 25 ns timing/triggering resolution and passes data from the I/O modules to the real time processor
I/O Modules	<ul style="list-style-type: none"> • Contains ADC DAC conversion circuitry • Built in signal conditioning 	Provides direct connection to sensors and actuators
FPGA chip	<ul style="list-style-type: none"> • 3M gates 	Executes the hardware implementation of the control logic, I/O, triggering and synchronization design

Figure 4.2: cRIO Component functionality.

a host computer running windows, and then Labview compiles and implements the code in hardware.

The Labview FPGA module enables the use of high level graphical data flow programming to create a highly optimized gate array implementation of analog or digital control logic to custom define I/O and control hardware circuitry. When a FPGA hardware is targeted such as a CompactRIO chassis or R Series intelligent DAQ device, the Labview programming palette is simplified to contain only the functions that are designed to work on FPGAs. The primary programming difference compared to traditional Labview is that FPGA devices use integer math rather than floating-point math. Also, there is no notion of multi threading or priorities since each loop executes in independent dedicated hardware

and does not have shared resources-in effect, each loop executes in parallel at “time critical” priority.

4.3 Application design

A typical real-time control application design has the following components with respective functionalities as depicted in Figure 4.3.

- Rio FPGA core application for input, output, communication, and control
- Time-critical loop for floating-point control, signal processing, analysis, and point-by-point decision making
- Normal-priority loop for embedded data logging, remote panel Web interface, and ethernet/serial communication
- Networked host PC for remote graphical user interface, historical data logging, and post processing

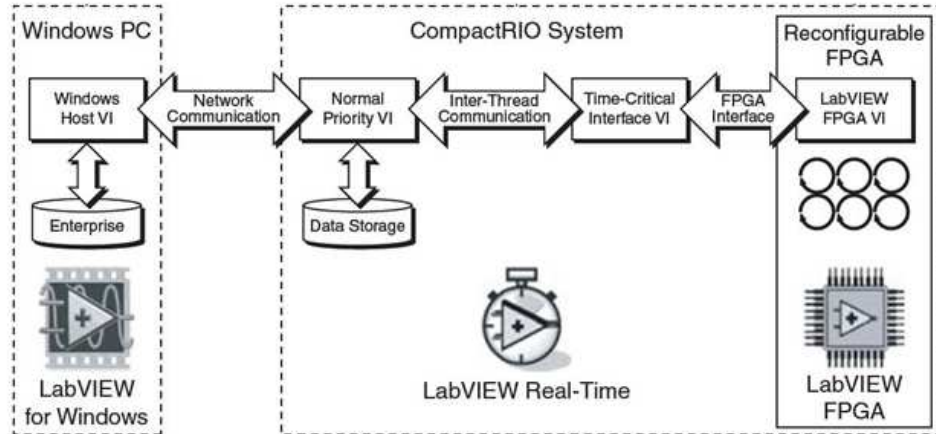


Figure 4.3: Typical application design.

Figure 4.4 gives the flow chart of the application design which was implemented with 5 major parts with the following subsections describing each.

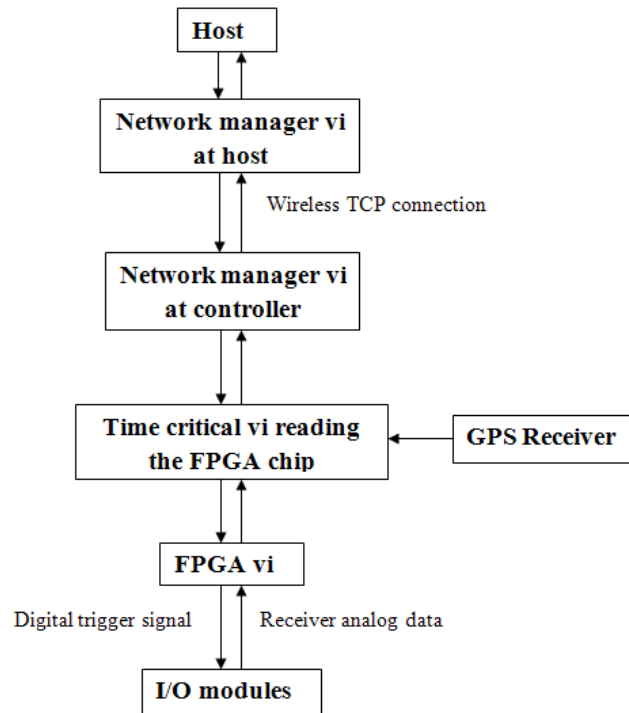


Figure 4.4: Flow chart of application design.

4.3.1 FPGA vi

As mentioned before, customized hardware is programmed in labview and then compiled and implemented in hardware. The FPGA vi is implemented in the FPGA chip which is embedded in the 8 slot chassis used. Its main purpose is to interact with the I/O modules in acquiring or producing a signal

The fpga vi, FPGA Rarces 1.vi (Appendix A.1) performs 3 functions,

- Simulates a 40ms, 17 % duty cycle digital signal at one of the digital module output pins (NI 9401). This is used to trigger the transmitter current signal which is in turn used to excite the transmitter coil.
- Samples the analog data from the receiver coils through the analog module (NI 9239).
- Evaluates the LSB weights and offsets of the analog module to convert raw data to calibrated data.

Fpga vis can be configured for direct memory access (DMA) which improves data transfers for high speed buffered data acquisition applications for compact rio devices. When the real time project is built, the target which needs to be programmed is selected and a FIFO is configured to implement DMA transfers. The present configuration of hardware can support 3 DMA channels. The only data type which is supported by FPGA FIFOs is unsigned 32 bit integers and the depth is decided on the rate at which data is written into the FPGA fifo and the rate at which the host can read from the fifo. The slower the real time host vi compared to the FPGA vi, the larger a fifo is needed, to avoid overflow and loss of data at any point of time.

4.3.2 Time critical loop vi

A time critical loop is generally used for FPGA read/write and floating point control. It is called a time critical loop because it should not be too fast or too slow to underflow or overflow the FPGA buffer respectively. The FPGA interface palette gives access to functions which can be invoked exclusively on the FPGA target. The time critical loop in the present project TCL crio master 9-4 chain single loop.vi(Appendix A.2) performs the following functions

- Reads the raw data from the FPGA fifo, converts into calibrated data using the module offsets and LSB weights and passes into an array.
- Reads gps data serially from the controller's serial port using VISA driver commands.
- Controls the 'USER1' LED light to update the user on the status of the controller

4.3.3 Normal priority loop

A normal priority loop vi is typically used for embedded data logging, web interface and ethernet or serial communication between the controller and the host computer. Being

known for its reliability and usage for large data transfers between the host and the controller, a wireless tcp connection was used for the present project. The normal priority vi, NPLcrio master 9 4 chain.vi (Appendix A.3) performs the following functions

- In the initialization loop, real-time FIFOs are created for 'start', 'stop' controls (host controls to be sent to the controller) and GPS data and receiver coil data (data to be sent back to host).
- A TCP listener is created at port 12344(default) which waits for the established tcp network connection.
- The boolean controls from the host (reader case) and the data to the host (writer case) are exchanged in two parallel case structures through 'RTCW send receive.vi'(library vi available with real time communication wizard tool).
- Time critical vi is called as a sub vi to run FPGA vi and read data from the modules.

4.3.4 TCP connection manager at the host side

Global variables are created for the start, stop controls from the host and the gps data from the controller. The present tcp connection manager, Hostcrio master 9 4-chain mod.vi(Appendix A.4) is very similar to the normal priority loop and it manages the TCP connection at the host side and performs the following tasks

- A TCP connection is opened with the IP address of the target and port (12344-default)
- Start and stop global variables are type cast into strings and passed onto RTCW send receive.vi which makes the writer case.
- In the reader case, the data array is read point by point and put in an array to be accessed in the host.

- The gps data which is acquired from the controller is assigned to a global variable to be read in the networked host(computer providing a real time analysis of the data)
- The tcp connection is closed once the controls are sent and the data is received.

4.3.5 Host vi

Host vi is the main interactive vi where the user selects to start the transmitter coil excitation followed by receiver coil data acquisition along with the GPS location of the sensor. It basically performs the following functions

- Sets values to the global variables, 'start' and 'stop' when the user chooses to start or stop the acquisition respectively
- Updates a spectrogram waterfall diagram to visualize the flow of data and keep a track of previous 10 seconds data visually
- Records and stores the analog data along with a gps tag in a binary file
- Presents the analog and gps data in real time on the front panel

4.4 GPS target tracking

A high precision trimble differential GPS system was used with a base station and a roving GPS receiver. Differential gps is an advanced form of gps where, extended accuracy is obtained by setting up the base station at a known location and made to acquire its location and the difference which is the error that is used to correct the roving receiver's location. The NMEA message used was 8 decimal points accurate giving a 2mm accuracy in position. The roving antenna was mounted on the robot along with the data acquisition hardware and the GPS data was synced with the real time receiver coil data so that every data point in the receiver signal is tagged with the exact GPS location of the receiver. Figure 4.5 gives a typical post processed data set of a single coil pair with tagged GPS data. It is the receiver coil data plot from Lane 1 with 7 targets from east to west, when overlapped with

the static GPS map for exact target mapping with the exact target position in latitude and longitude. The post processing of data and methods used is explained briefly in the next chapter.

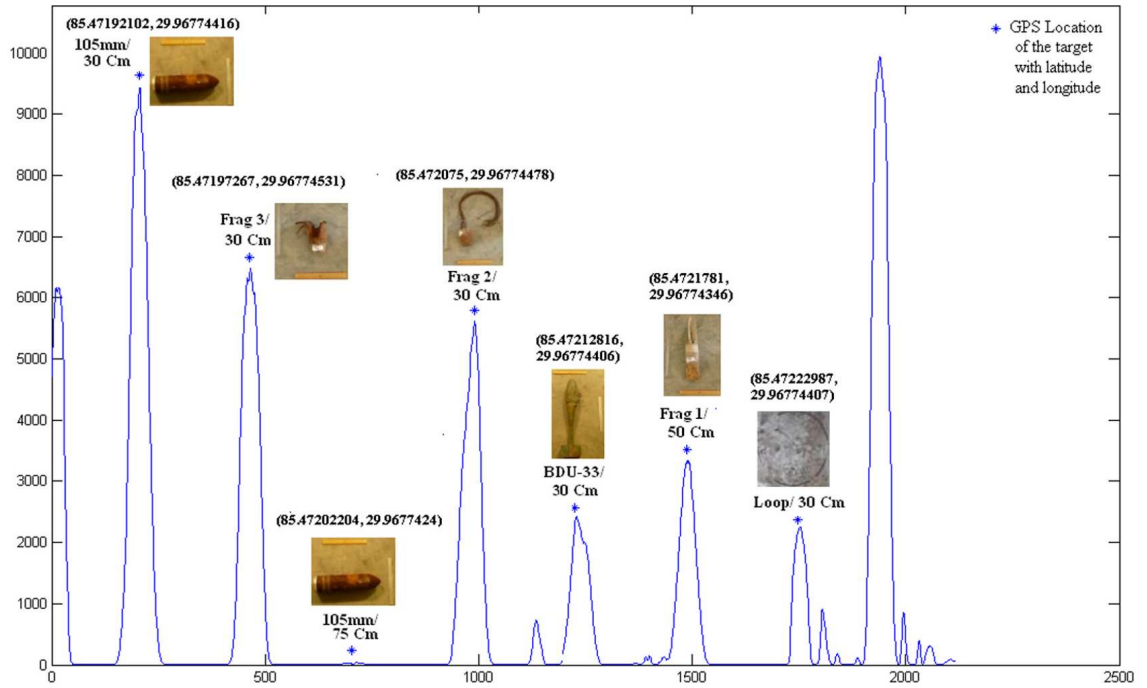


Figure 4.5: Sample receiver coil data.

The wired ethernet connection used during the initial stages of sensor development was replaced by a 802.11 wireless router and modem to transmit data to and from the networked PC. The use of wireless gave more mobility and access without any human interaction near the test site area.

CHAPTER 5

MEASUREMENTS AND RESULTS

In the present chapter, the measurements and post processing of data collected at the Eglin Air Force Research Laboratory, Florida are presented. The plots of the 3 configurations of the receiver coils are discussed to validate the capabilities of the EMI sensor as a good detection device.

5.1 AFRL measurements

The main purpose of the tests was to demonstrate the detection capabilities of the pulsed EMI sensor. These tests were Conducted in December 2008 for 5 days at Eglin air force base along with a team of 4 from ERDC, Mississippi. The runs were dynamic along 5 equidistant lanes from west to east with 32 buried diffused ferrous and non ferrous targets. Figure 5.1 gives the test area layout with the static GPS locations marked as asterisks. Appendix D gives the details of the nature and depths of all the targets. The beginning and end of every lane was marked with a long pair of angle iron which served as fiducials. Each test run was done from west to east on lane 1, following a serpentine path on the other lanes, and concluding it from east to west on lane 1, as shown in the path in Figure 5.1. Three coil configurations with 1,2 and 4 arrays of receiver coils were used as described in chapter 3 with 3 runs of data collection each time. Static GPS data of all targets was collected to verify the test results with respect to the target GPS tagging.

5.1.1 Post processing of data

Each data set in each run consisted of a continuous signal at the receiver coil from a single lane. It can be imagined as continuous smaller data sets of 40ms each(transmitter

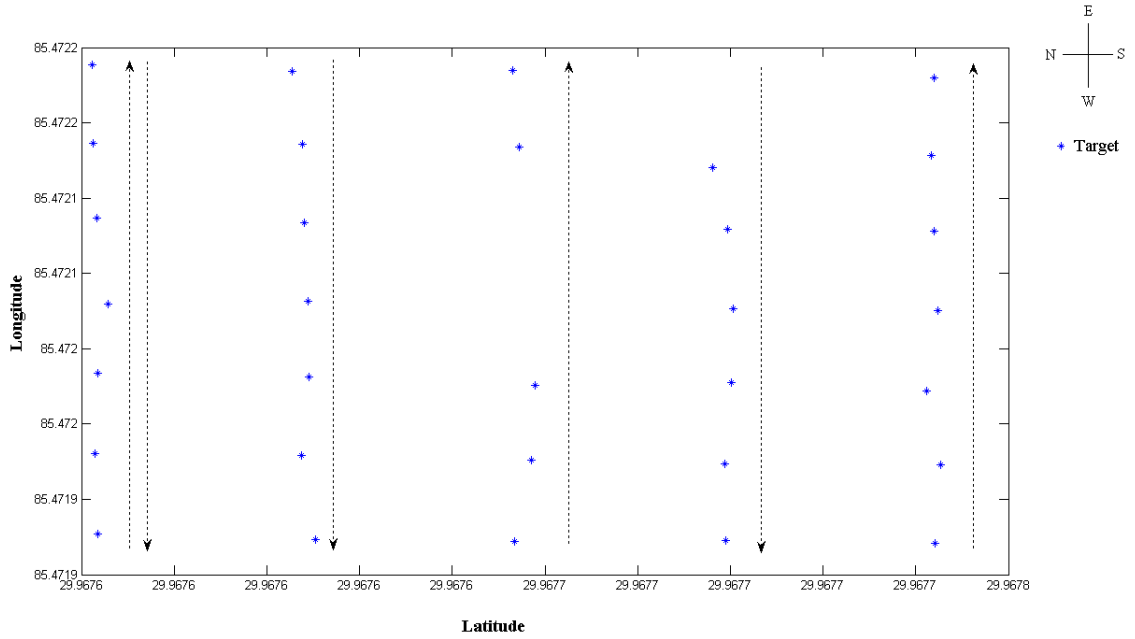


Figure 5.1: Target position and robot trajectory.

current pulse time period). A background shot called the baseline signal is chosen for each data set where there is no target, this was done by plotting the entire set and then choosing a point where there was minimum receiver response. This background data shot is then subtracted from all other shots to reduce noise and enhance the target response captured. The object coupled receiver energy is then computed and plotted as a 3D plot with the respective GPS locations. This 3D plot is super-imposed with the actual static GPS 2D grid to verify if the targets were located accurately with respect to the GPS locations, as shown in Figure 5.2. This gave an idea of where exactly the receiver signal was at a peak with respect to the real known locations of the targets. This method not only proved the sensor's detection abilities but also GPS location tagging abilities.

5.1.2 GPS correction

The GPS antenna was placed in the cart on the segway and since the location of the receiver coil is needed, a correction needs to be applied to the longitude of the acquired GPS data. This correction in appendix c is based on Haversines formula which calculates

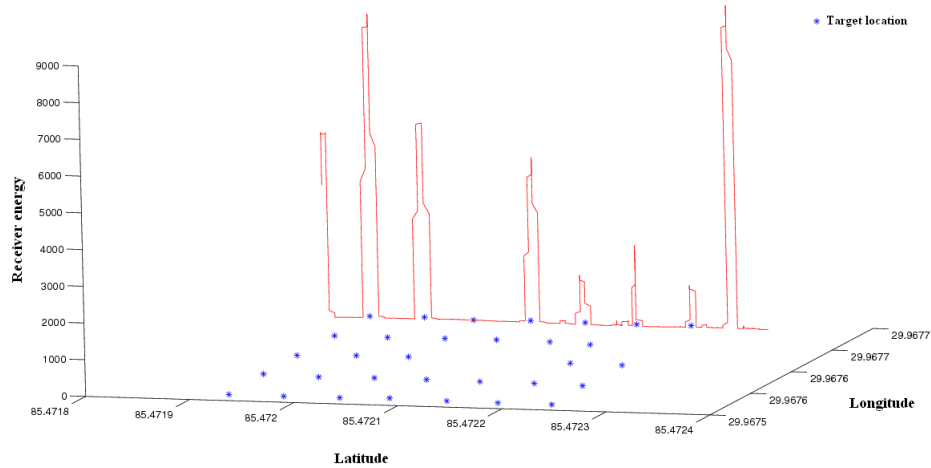


Figure 5.2: Superimposition of static GPS map on the data plot for position tracking.

the distance between 2 points when lat lon is known. The formula has less error when the distance between two points is less[11]. It can be applied by knowing the exact distance between the antenna and the center of the coil. All the data plots were analyzed manually and detection capability being the main purpose of the experiments, GPS correction was not applied to the presented results. To tag the GPS location of the coil accurately, this correction would need to be implemented.

5.1.3 4 coil array results summary

The three coil configurations used as described in chapter 3, worked as a differential system with a null signal when the coil pair was centered on the target. The following subsections summarize the results with a few sample plots. A summary of a single run is provided since all runs had similar responses. All these plots are provided in APPENDIX.

The first used was a 4 receiver coil array with dual-coil receiver units in a bucking configuration. Figure 5.3 shows a typical post processed data plot for a 4 coil pair configuration receiver coil. The following is a summary of results of the four coil pair array receiver configuration.

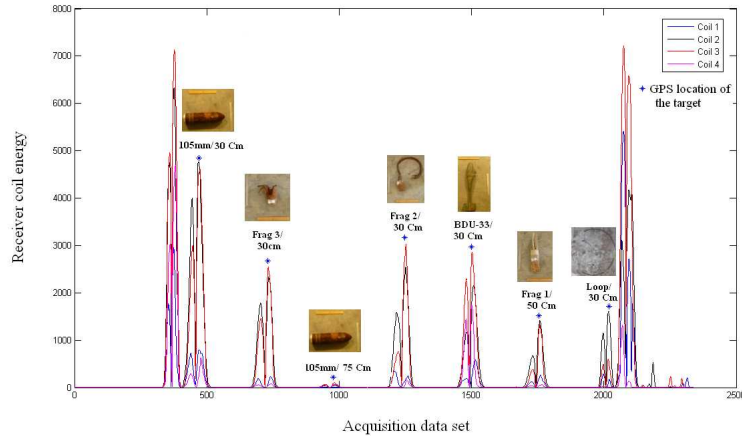


Figure 5.3: Sample 4 coil pair receiver coil data of lane 1.

- Lane 1: All 7 targets were detected and the deepest target, 105mm at 75cm had a relatively small but significant response.
- Lane 2: All 6 targets were detected and the deepest target, 105mm at 120cm(3.93 ft) depth showed a small but identifiable response.
- lane 3: 4 out of 5 targets were detected with smaller responses from fragment at 30cm depth and loop at 30cm depth. The sensor missed detecting frag3 at 50cm.
- Lane 4: 5 out of 7 targets were detected and missed two 105mm targets, 120cm deep.
- Lane 5: all the targets were detected
- Lane 1 in E-W direction: All targets were detected with relatively smaller but significant response from the 105mm target, 75cm deep.

Typically all the targets and the fiducials were detected except two 105mm targets, 120cm deep targets in lane 4 and a fragment, 50cm deep in lane 3. Four runs were taken with the 4 coil configuration and 3 of them showed identical responses. The data collected for Run 2 showed a lag of GPS data in time and the data could not be tagged with target GPS locations, but the responses were similar to the other runs.

5.1.4 2 coil array results summary

The following is a summary of results of run 1 of two coil pair array receiver coil. Coil 1 was aligned with all odd numbered lanes and coil 2 was aligned with all even numbered lanes. As it can be observed from the plots in Appendix D, coil 1 response is greater than coil 2 response for odd numbered lanes and vice versa for even numbered lanes. Figure 5.4 gives a typical response plot using a 2 coil pair receiver configuration of lane 1 east to west.

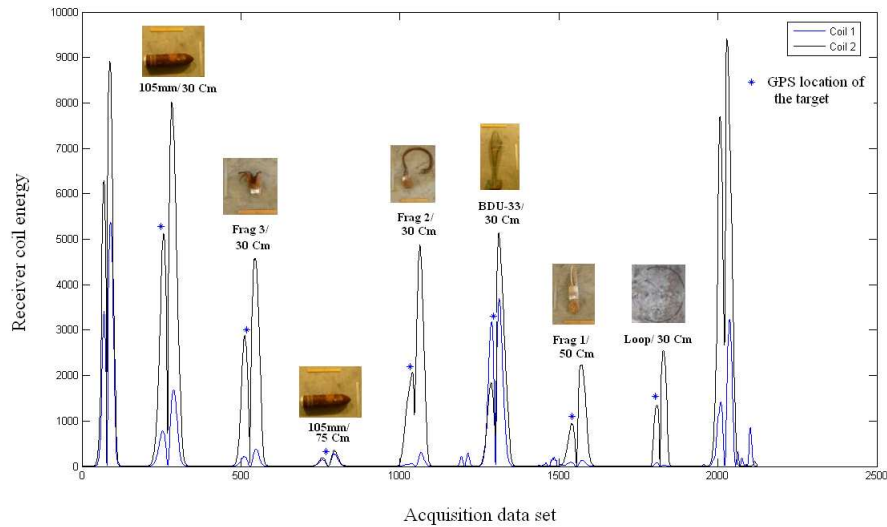


Figure 5.4: Sample 2 coil pair receiver coil data of lane 1.

- Lane 1: All 7 targets were detected and the deepest target, 105mm at 75cm had a relatively small but significant response.
- Lane 2: All 6 targets were detected and the deepest target, 105mm at 120cm(3.93 ft) depth showed a small but identifiable response.
- lane 3: All 5 targets were detected with smaller responses from fragment at 30cm and 50 cms depths. The sensor's response from a fragment at 50cms depth was very small but good enough for a detection purpose.
- Lane 4: 5 out of 7 targets were detected and missed two 105mm targets, 120cm deep.

- Lane 5: all the targets were detected
- Lane 1 in E-W direction: All targets were detected with relatively smaller but significant response from the 105mm target, 75cm deep.

2 coil and 4 coil configurations had similar responses and the 2 coil configuration was able to detect a target in lane 3 which was missed by the 4 coil configuration.

5.1.5 1 coil pair results summary

The following is a summary of results of the one coil pair receiver configuration.. Figure 5.5 gives a sample plot.

- Lane 1: All 7 targets were detected and the deepest target, 105mm at 75cm had a relatively small but significant response.
- Lane 2: 5 out of 6 targets were detected. Missed detecting 105mm target 120 cm deep
- lane 3: All 5 targets were detected.
- Lane 4: 6 out of 7 targets were detected. Missed detecting a 105mm target 120cm deep but was able to detect 105mm heat target 120cm deep.
- Lane 5: all the targets were detected
- Lane 1 in E-W direction: All targets were detected with relatively smaller but significant response from the 105mm target, 75cm deep.

Figure 5.5 gives the success map of all the coil configurations summarizing the above results. The colored box against a target indicates the success of detection. It shows that all targets except a 105 mm target, 120cm deep were detected with one or the other receiver configuration.

Overall all the configurations with the proposed hardware proved to be good detection setup and it can be observed from the plots that receiver signal power response of 4 coil

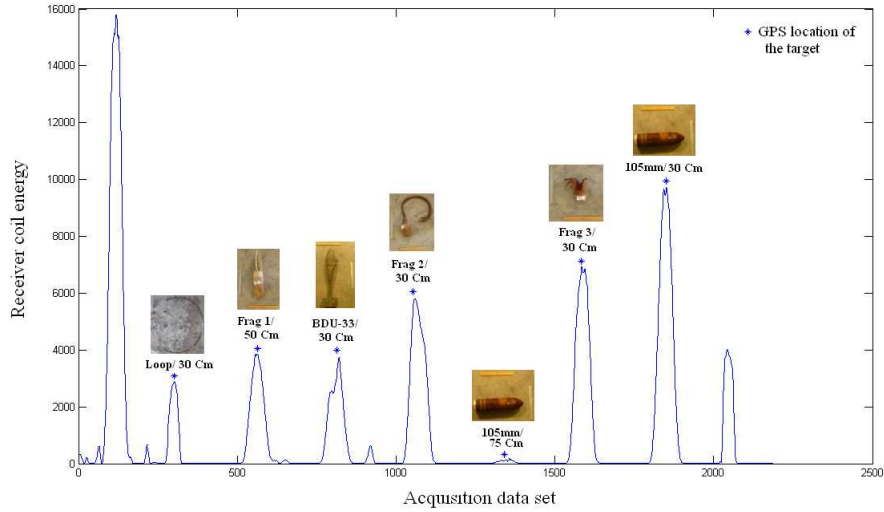


Figure 5.5: Sample 1 coil pair receiver coil data of lane 1.

configuration was slightly more than the 2 coil configuration and the least was of the 1 coil configuration. 1 coil configuration's power response being low and as explained in section 3.4 might not prove to be an optimal design since a target passing between the coil pairs will go undetected.

Position							
7	AFRL 105 30cm	ERDC Item 6 30cm	ERDC Item 9 50cm	AFRL 105 120cm	AU Loop 16-15 30cm		
6	ERDC Item 3 30cm	AFRL 105 HEAT 75cm	ERDC Item 8 30cm	AU Loop 19-15 30cm	ERDC Item 15 30cm		
5	AFRL 105 75cm	ERDC Item 5 30cm	AFRL BDU 33 120cm	ERDC Item 12 50cm	AFRL 57 30cm		
4	ERDC Item 2 30cm	AFRL 105 30cm	Dug and Refilled	ERDC Item 11 30cm	AFRL BDU 33 75cm		
3	AFRL BDU 33 30cm	ERDC Item 4 30cm	Dug and Refilled	AFRL 105 HEAT 120cm	ERDC Item 14 50cm		
2	ERDC Item 1 50cm	AFRL 105 120cm	AU Loop Fe-15 30cm	ERDC Item 10 30cm	AFRL 105 30cm		
1	AU Loop 12-15 30cm	Dug and Refilled	ERDC Item 7 30cm	AFRL 105 75cm	ERDC Item 13 50cm		
	1	2	3	4	5		
			Lane				

■ 4 coil pair detection success ■ 1 coil pair detection success
■ 2 coil pair detection success ◆ Empty

Figure 5.6: Detection success map

CHAPTER 6

CONCLUSION

In this thesis, a summary was provided on the development of a time domain EMI sensor with primary objective of detection capability. Chapter 3 provided a detailed description of the hardware circuitry involved followed by chapter 4 giving an in depth understanding of the data acquisition system used. From the experiments done at Eglin AFRL, Florida and the data presented, the overall system proved to be a good detection device with successful target detection along with accurate GPS location tagging. The different configurations of receiver coils helped to provide an understanding of the detection capabilities of the system. The single coil pair proved to be the least sensitive of all configurations and had the additional disadvantage of not detecting targets passing under the centerline of the array.

The fiducial and cart which were used as the lane markers should have been placed further away from the first targets in the lanes so as not to interfere with detecting other targets. Further up gradation of the data acquisition equipment to meet wireless needs (with availability of new wireless DAQ cards) can prove to be useful and reduce the risk of having a disconnection and thus loss of data. Better amplifying and signal processing techniques can be employed to boost a signal from deeply buried objects. Some of the 105mm targets at 120cm(3.9ft) were detected but with a weak signal and in some cases they were not detected.

The receiver coil amplifier was redesigned to improve dynamic range so as to enhance the sensor's discrimination capabilities. A further improvement in the receiver amplifier circuitry might improve the dynamic range to 6 orders of magnitude compared to the improvements already achieved.

BIBLIOGRAPHY

- [1] *Report Of The Defense Science Board Task Force On Unexploded Ordnance*, December, 2003 available on line at <http://www.acq.osd.mil/dsb/reports.htm>
- [2] *Report Of The Defense Science Board Task Force On UXO clearance, Active Range UXO Clearance, and Explosive Ordnance Disposal Programs*, April, 1998 available on line at <http://www.acq.osd.mil/dsb/reports.htm>
- [3] F.S. Grant and G.G. West, *Interpretation Theory in Applied Geophysics*, New York: McGraw-Hill Book Company, 1965.
- [4] C.E.Baum, *Detection and Identification of visually observed targets*, Taylor and Francis, 1999(Chapter 6).
- [5] Claudio Bruschini, *A multidisciplinary analysis of frequency domain metal detectors for humanitarian demining*. Doctoral thesis, Vrije Universiteit Brussel, 2002.
- [6] Carl Nelson. Simultaneous time-domain and frequency-domain metal detector. U.S. Patent #7078906, 18 Jul. 2006.
- [7] K.B.Lloyd, *Design and construction of a pulsed electromagnetic induction system for unexploded ordnance detection and discrimination*, Master's Thesis, Auburn University, 2004.
- [8] C.A. Balanis, *Advanced Engineering Electromagnetics*. New York: John Wiley and Sons, Inc, 1989.
- [9] J.N.Palasagaram, *Efforts towards the design and development of an electromagnetic induction sensor optimized for detection and discrimination of unexploded ordnance*, Master's Thesis, Auburn University, 2006
- [10] "LT1028 spec sheet" available on line at <http://cds.linear.com/docs/Datasheet/1028fa.pdf>.
- [11] Haversines formula available on line at <http://www.torontohealthprofiles.ca/documents/resources/Methods.pdf>

APPENDIX A

DATA ACQUISITION LABVIEW CODE

This section gives a description of the graphical software code of the data acquisition modules described in chapter 4.

A.1 FPGA vi

Figure A.1 shows the block diagram of the FPGA vi which is coded using special labview FPGA palette functions.

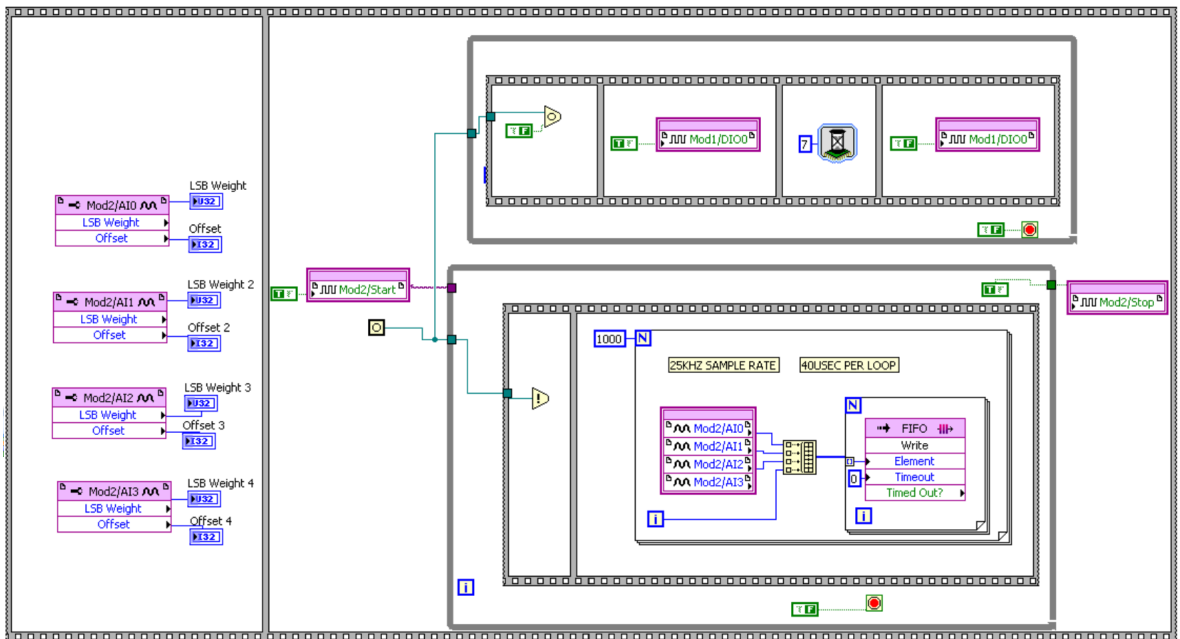


Figure A.1: FPGA vi

A flat sequenced structure is used in the present FPGA vi, the first pane reads the offsets and calibration constants. The second pane consists of 2 synchronized parallel loops, where one loop samples the data from the 4 channels of the analog module. The resulting 24

bit are combined into an array and passed into a 'for' loop. The 'for' loop indexes through each element and passes the data into the DMA FIFO. The other while loop generates a 40ms pulse of 17% duty cycle for the purpose of triggering.

A.2 Time critical loop vi

A time critical loop is generally used for FPGA read/write and floating point control. Figure A.2 gives the block diagram of the time critical loop. The present vi has 2 nested time loops with a case structure enclosing the inner timed loop in the true case. The select terminal is wired to the read control which decides the execution of the time critical logic. Real time communication wizard (Tools\Real-Time module\Communication Wizard) is used where it converts an existing real-time vi into a client server architecture. Controls and indicators in the time critical code are replaced with real time FIFOs that transfer data to a parallel lower- priority communication loop

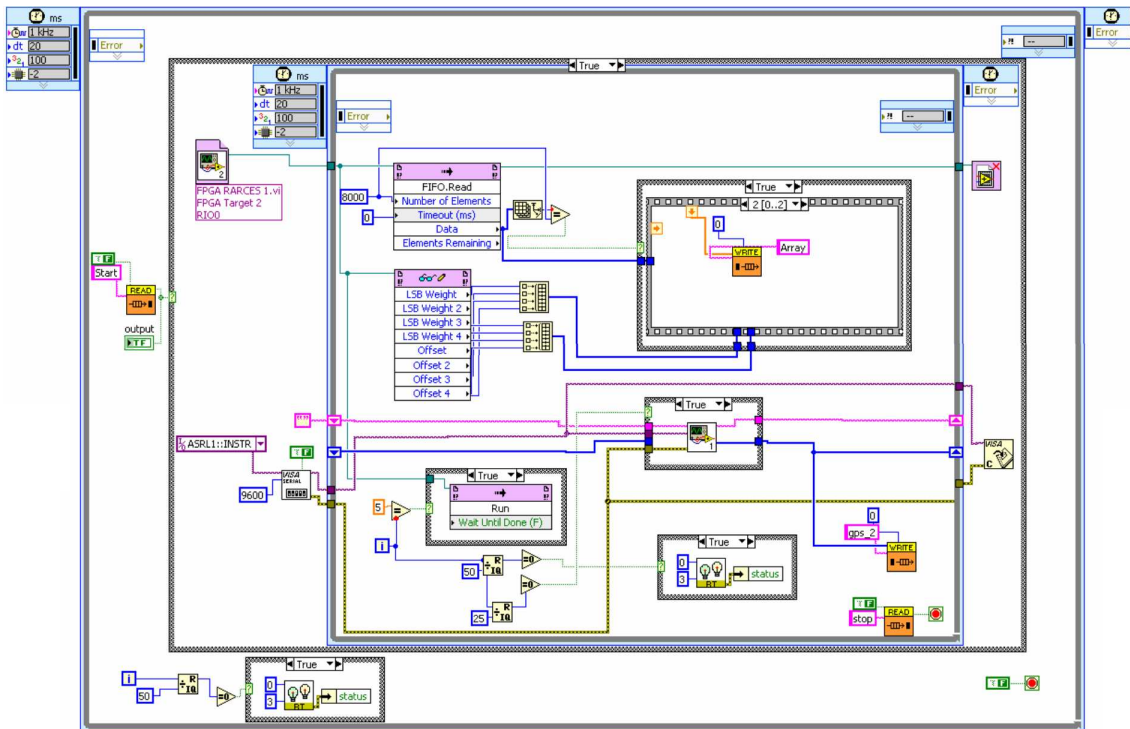


Figure A.2: Time critical loop vi

A reference of the target FPGA vi is opened and a “run” method is invoked to run the vi, subsequently other functions are invoked depending on the functionality required and the reference is closed once data is read. A “read” method and a “read/write control” are called on the reference of the FPGA vi to read the analog data and the values of the LSB weights and offsets from the indicators of the FPGA target respectively. These data values along with the bundled offsets are used in one of the cases in a stacked sequence structure to convert raw data into calibrated data. The converted data is reshaped into a single array and written into a real time communication wizard FIFO in the following two cases. A serial port on the micro controller was used as an input for the GPS signal. “VISA configure serial port” function gives a list of all the serial ports available and a port of interest is selected with a specific baud rate. A case structure is used with 'RARCES GPS' sub vi to strip the "GPGAA" stream of the GPS signal to get the latitude and longitude along with the time stamp, then it is passed onto a RTCW FIFO just like data is sent. The Boolean at the selector terminal of the case structure is true every second and GPS data is updated accordingly. The GPS data is fetched if the loop count of the main while loop is divisible by 25 which is logical considering that each loop is 40ms by virtue of the trigger and 25 loops account for 1 second when GPS data is updated.

RT LEDs.vi form the real time library and is used to manipulate the LEDs on the controller. A blinking light on the 'User1' LED means the target is ready for use.

A.3 Normal priority loop vi

As mentioned earlier, a normal priority loop vi is used for embedded data logging, web interface and Ethernet/ serial communication between the controller and the host. The block diagram of NPL is shown in Figure A.3. It has an initialization loop followed by a case structure to read and write controls and data back and forth between the networked PC and the controller.

The initialization loop on the left hand side is a case structure which creates FIFOs for the start and stop global controls variables(which are boolean, named 'start' and 'stop')

and FIFOs for the data arrays with GPS and receiver coil voltage signals(named, 'gps2' and 'array'). The right hand case structure has 2 nested while loops to continuously read and write data. The outer loop manages the TCP connection by invoking a TCP listen function on the port(default 12344) before managing the data and closed once its done. The two case structures in the inner nested while loop are named reader case(uses RTCW from host) and writer case(uses RTCW to host), since the controls from the host pc are being read, they go into the reader case and the data which is being acquired is being written, it goes into the writer case. All the variables are managed using the real time communication wizard (RTCW) which is a tool readily available to manages all the variables involved in communication between the host PC and the controller.

Parallely TCL vi is called as a sub vi to read data continuously from the FPGA vi.

A.4 Network manager at host PC

'Hostcrio master 9 4-chain mod.vi' in the project files is the network manager at the host PC. Figure A.4 gives the block diagram of the vi. It is similar to the network manager at the controller(normal priority loop) described in the previous section. A 'tcp open connection' function is used to establish a tcp connection with the RT target specified by the IP address. The stop and start global variables which form the writer case(which form the reader case in NPL) are typecast into strings and the data(receiver voltage and GPS data) is unflattened from string into respective data types. It can be observed that the 'real time communication wizard send receive vi' manages the data at the host PC side too.

A.5 Host vi

The host vi as explained in section 4.3.5, performs 3 functions parallely using 3 while loops. Figure A.5 gives the logic for updating a spectral waterfall diagram to visualize and analyze data in real time. If observed from left to right, the data queue is obtained along with a notifier to pass it between parallel loops. Obtain notifier returns a reference to the notifier which is used later to obtain data when notification is sent. The start and

stop controls are assigned to global variables which can be accessed by any vi or sub vi. In the main while loop seen, a send notification function is used to send a message to the parallel loops and elements are dequeued and reshaped to separate 4 channel data for manipulation. 'sum n chain vi' computes the sum of object coupled voltages and multiplied with sensitivity of spectral waterfall chosen by the user. The spectral waterfall color can be chosen to represent sensitivity of the receiver.

Figure A.6 shows the logic for record and display options. The top loop obtains the data as a notification when the notifier in the above discussed loop sends a notification. This data is bundled with GPS data which is accessible as a global variable and written into a binary file. All this logic takes place when the user selects to record the data in the front panel. The bottom loop is similar to the record logic when the user selects the display option on the front panel. The data is presented as a waveform and GPS data as an unbundled cluster on the front panel.

The notifier and queue references after the data is obtained.

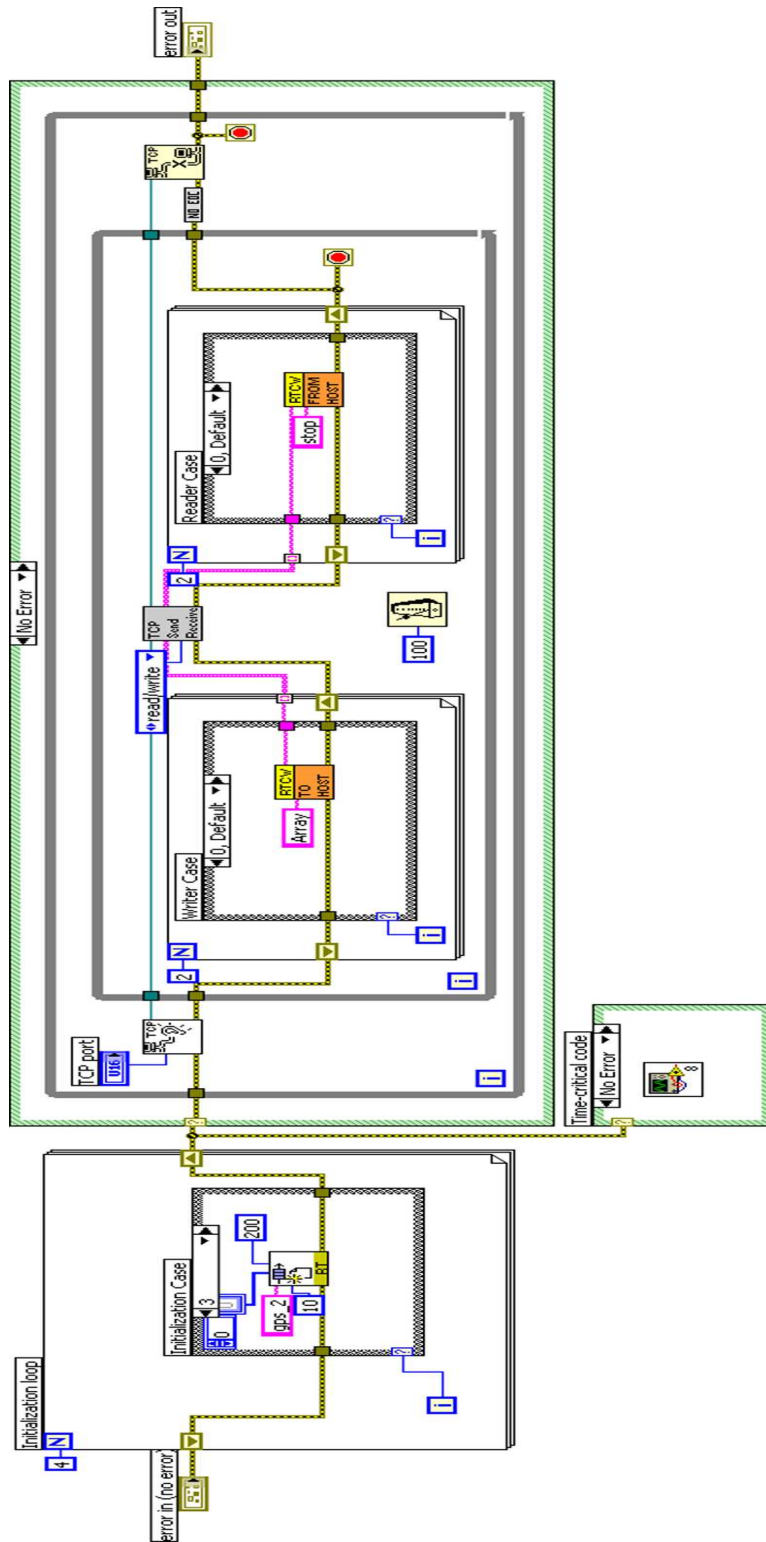


Figure A.3: Normal priority loop vi

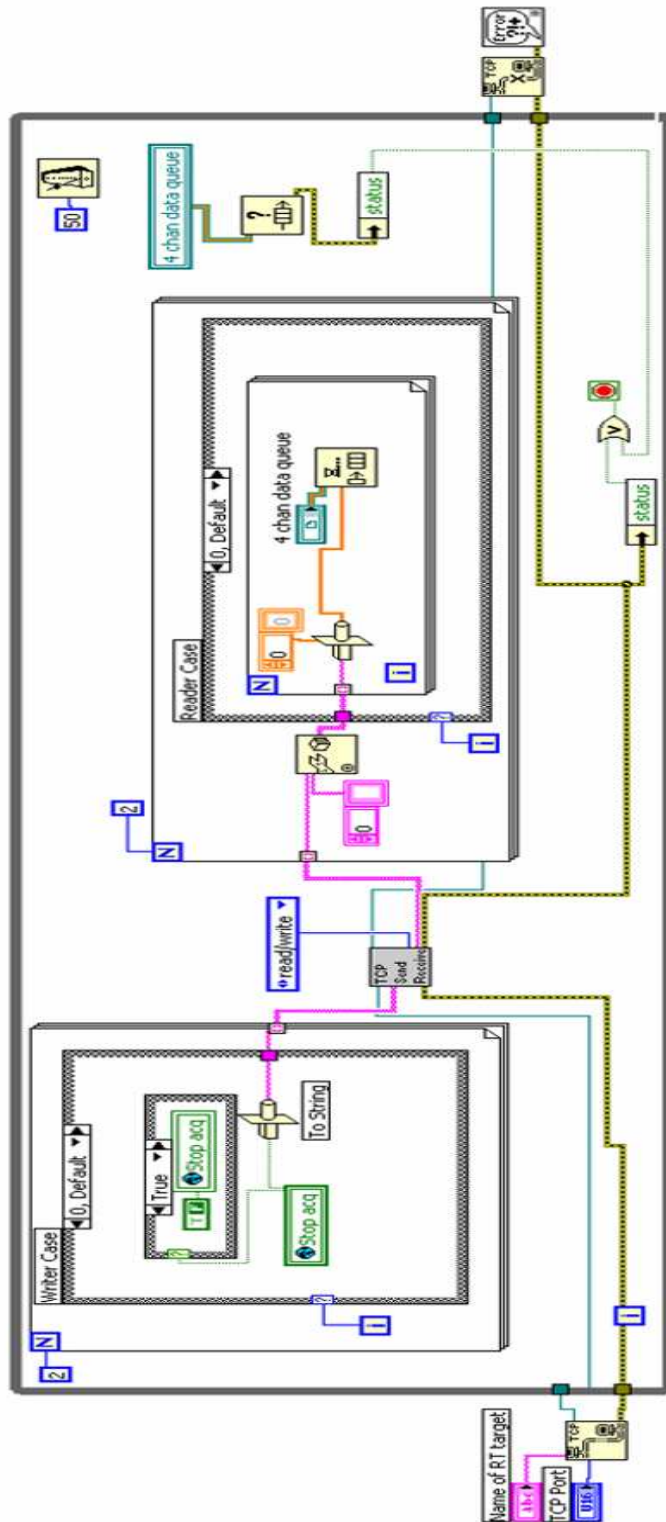


Figure A.4: Network manager at host PC

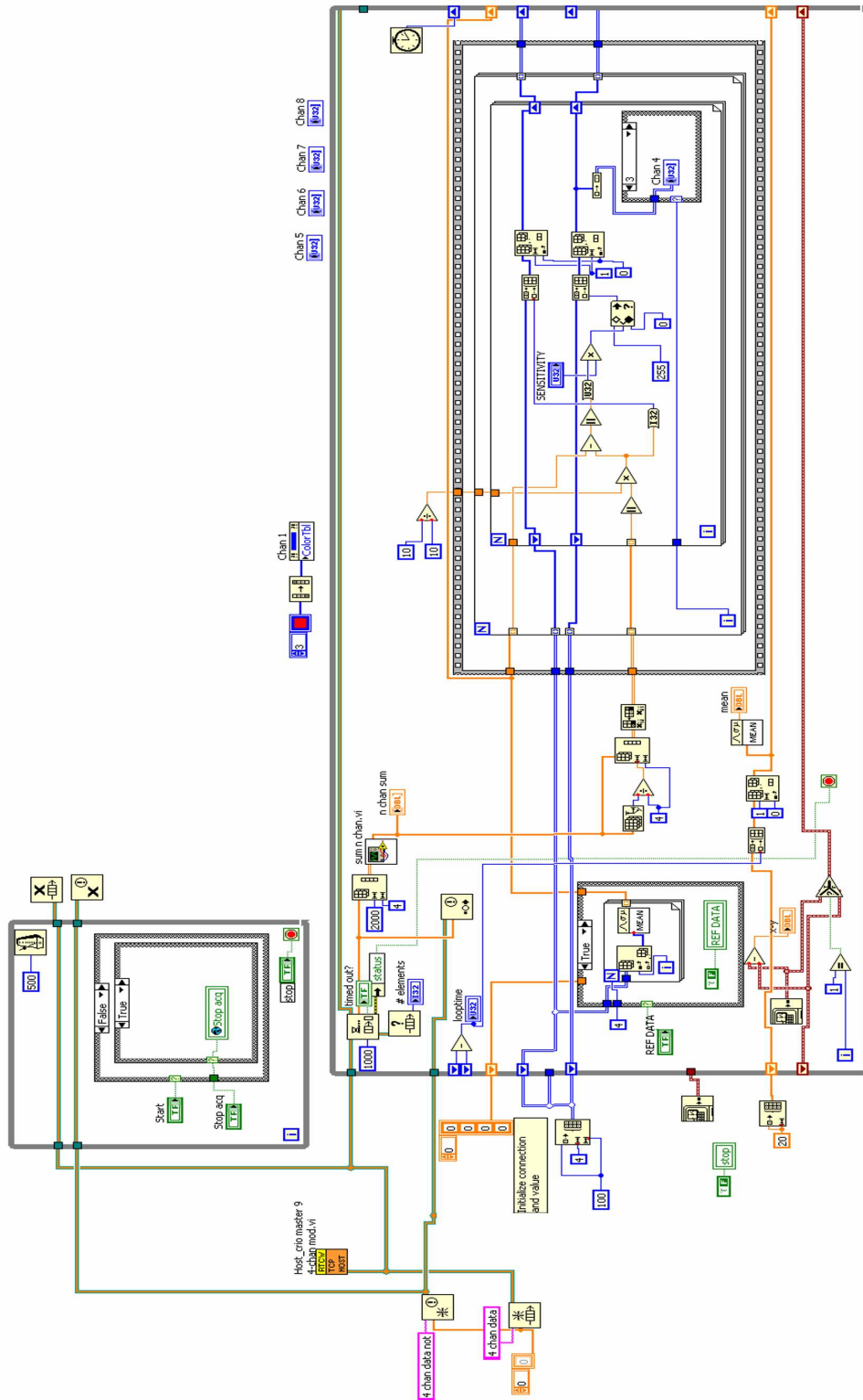


Figure A.5: Spectrogram waterfall logic

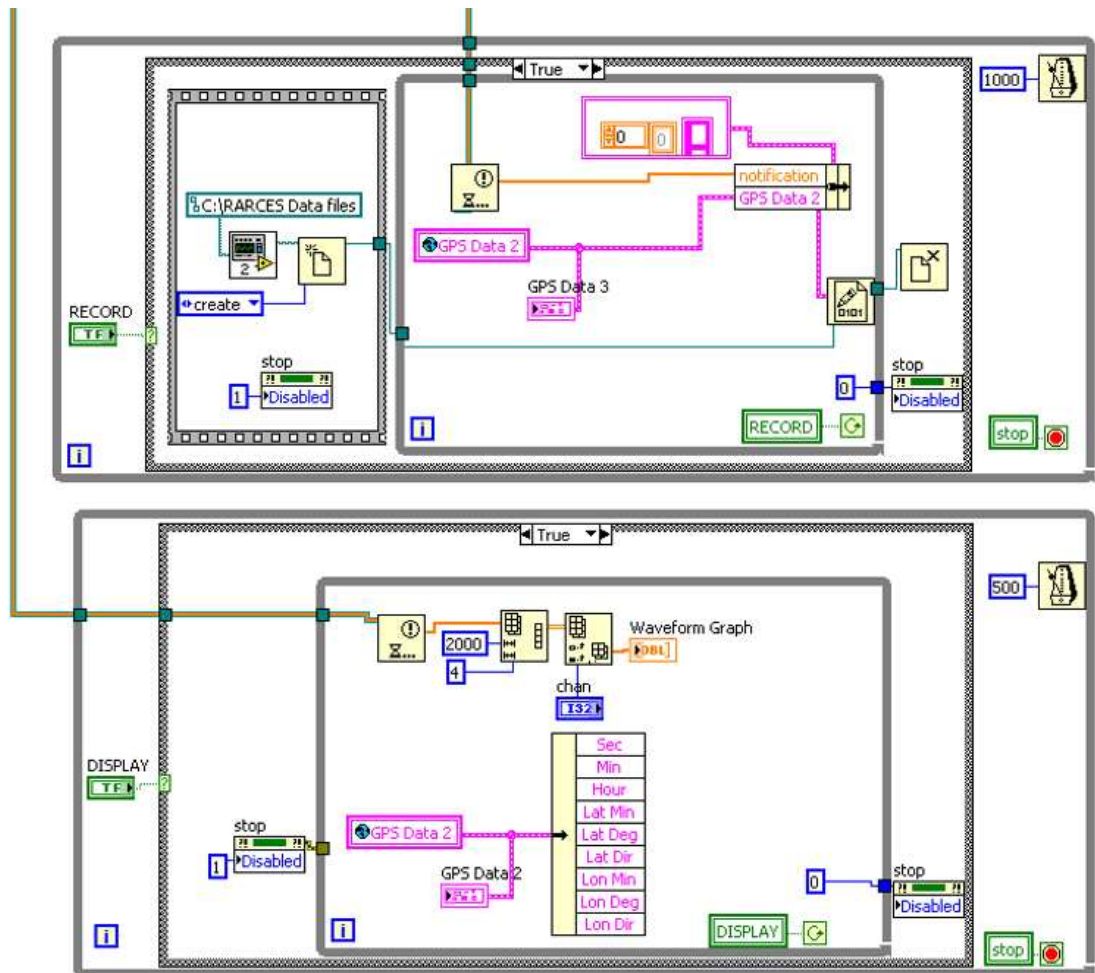


Figure A.6: Host record and display logic

APPENDIX B
GPS CORRECTION

The following correction formula is based on 'Haversine formula' which is used in navigation using great circle distances between two points on a sphere from their latitude and longitudes.

Using the following convention for sign,

$$LonP = lonP(west); Lonp = -lonP(east)$$

$$Latp = 90 - latP(North); Latp = 90 + latP(west)$$

If 2 points are located by A(Lat 1, Lon1) and B(Lat2,lon2)

$$dlon = lon2 - lon1$$

$$dlat = lat2 - lat1$$

$$A = \sin^2(dlat/2) + \cos(lat1) * \cos(lat2) * \sin^2(dlon/2)$$

$$c = 2 * \arcsin(\min(1, \sqrt{a})) \quad d=R*c$$

R is the radius of the earth and by solving for c in radians, distance between the points can be known. This formula can be applied to the present GPS correction to know the coordinates of the coil if coordinates of antenna and the distance between the coil and the antenna are known.

Since, the segway is moving East to west with approximately constant latitude, Lat A = Lat B and LonB can be solved by the known acquired GPS coordinates and the physical distance d which is the distance from the gps antenna to the center of the coils.

The error in Longitude can be calculated and rectified in realtime to know the exact location of the coil.

APPENDIX C

TARGET LIST AND REPRESENTATION

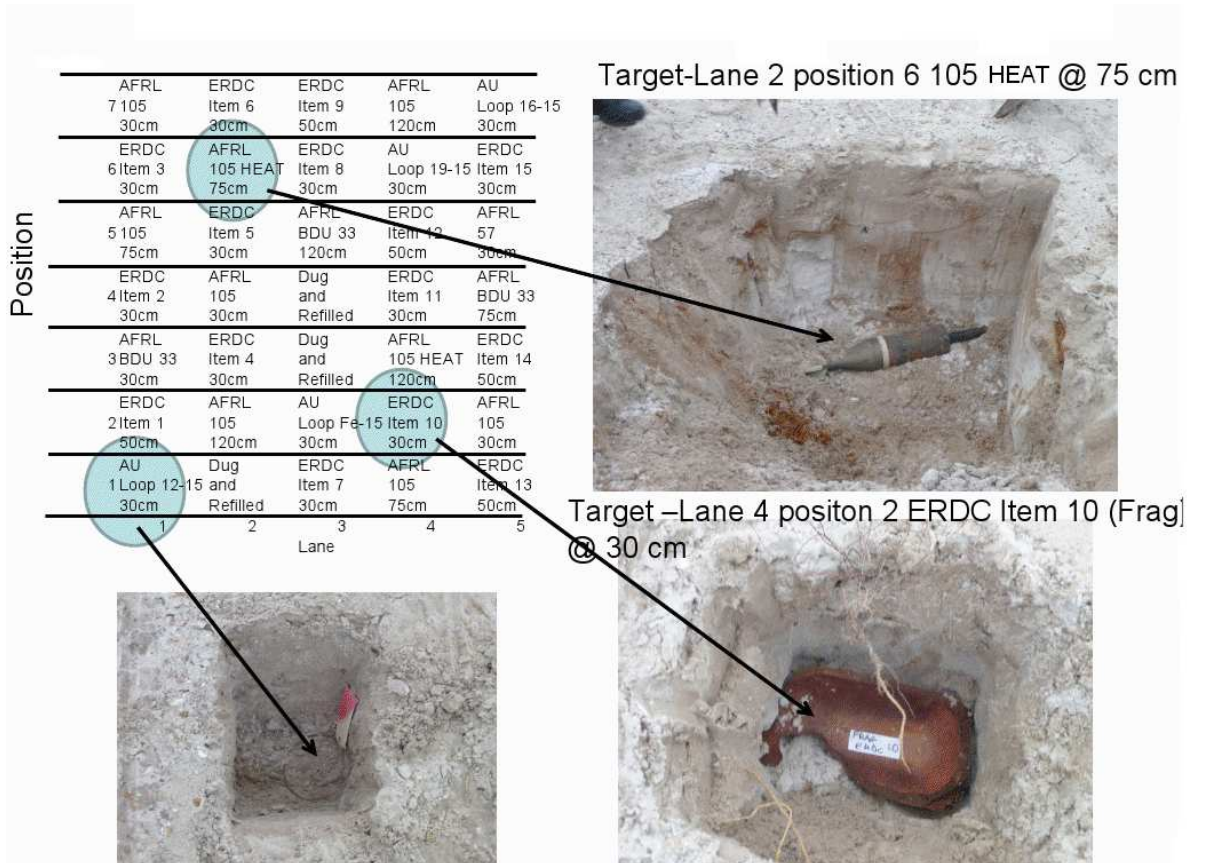


Figure C.1: Target list and representative targets used in AFRL tests.

APPENDIX D
AFRL DATA PLOTS

The following are the plots of AFRL measurements of a single run of all receiver coil configurations.

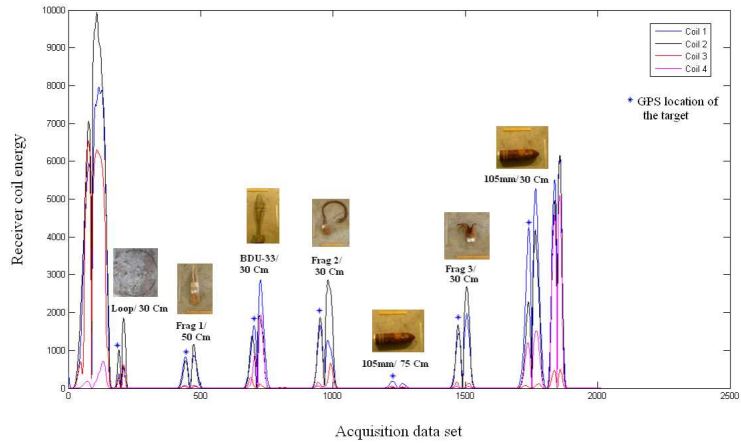


Figure D.1: 4Coil array response run1 lane1 west to east.

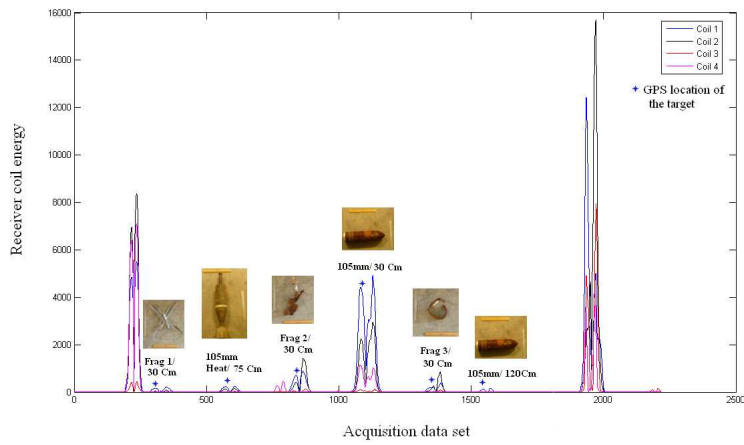


Figure D.2: 4Coil array response run1 lane2 east to west.

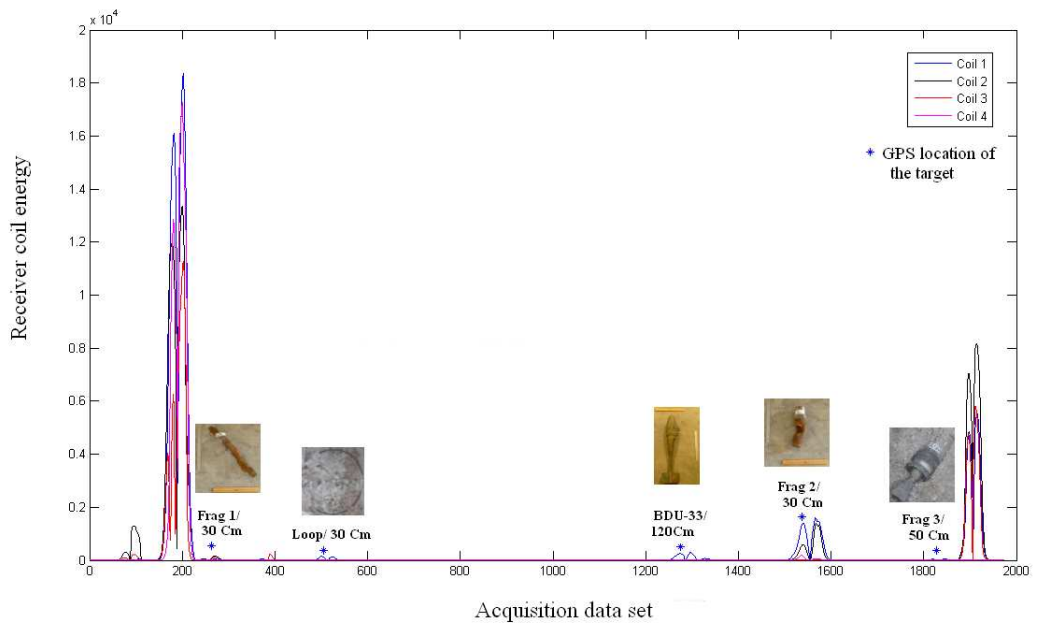


Figure D.3: 4Coil array response run1 lane3 west to east.

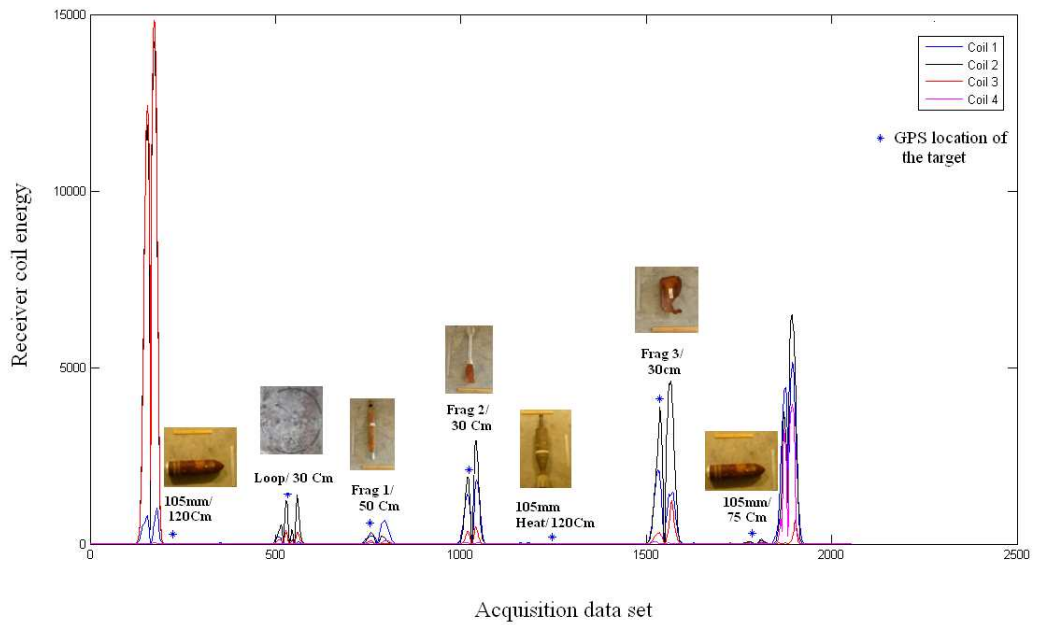


Figure D.4: 4Coil array response run1 lane4 east to west.

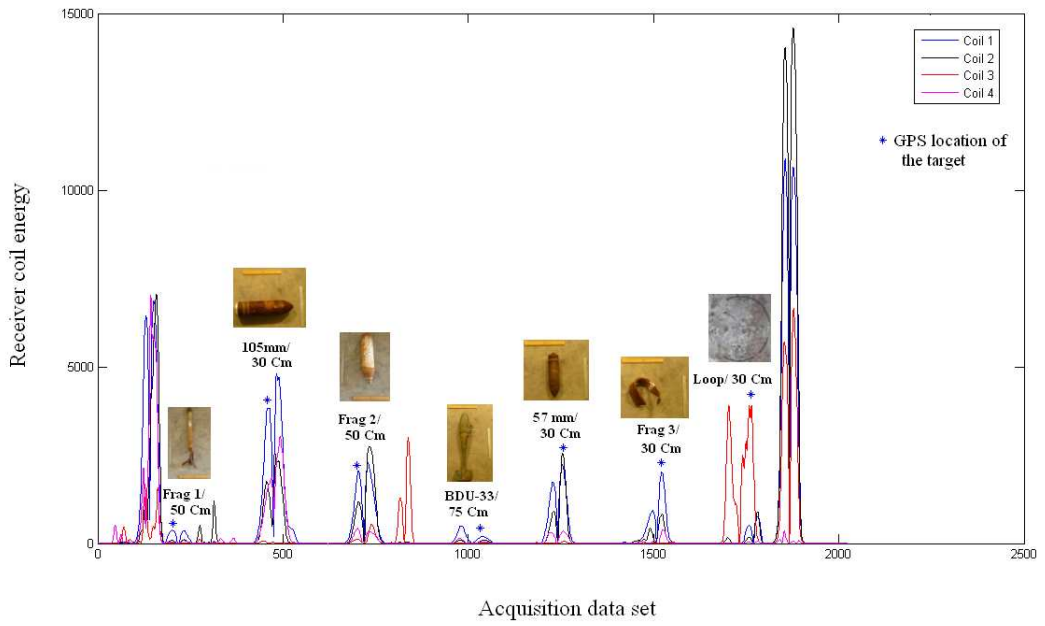


Figure D.5: 4Coil array response run1 lane5 west to east.

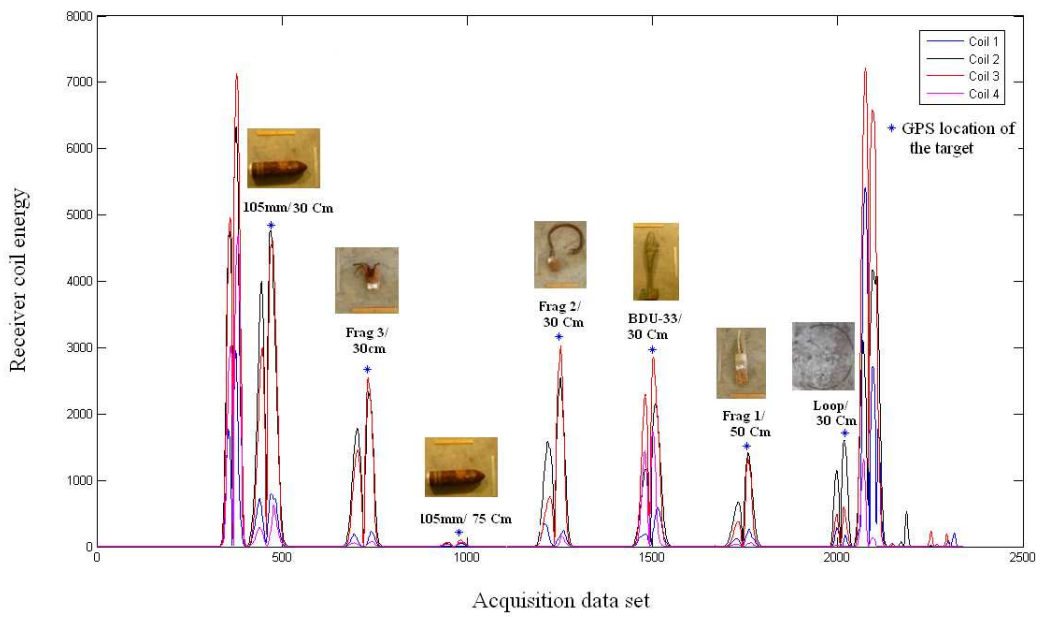


Figure D.6: 4Coil array response run1 lane1 east to west.

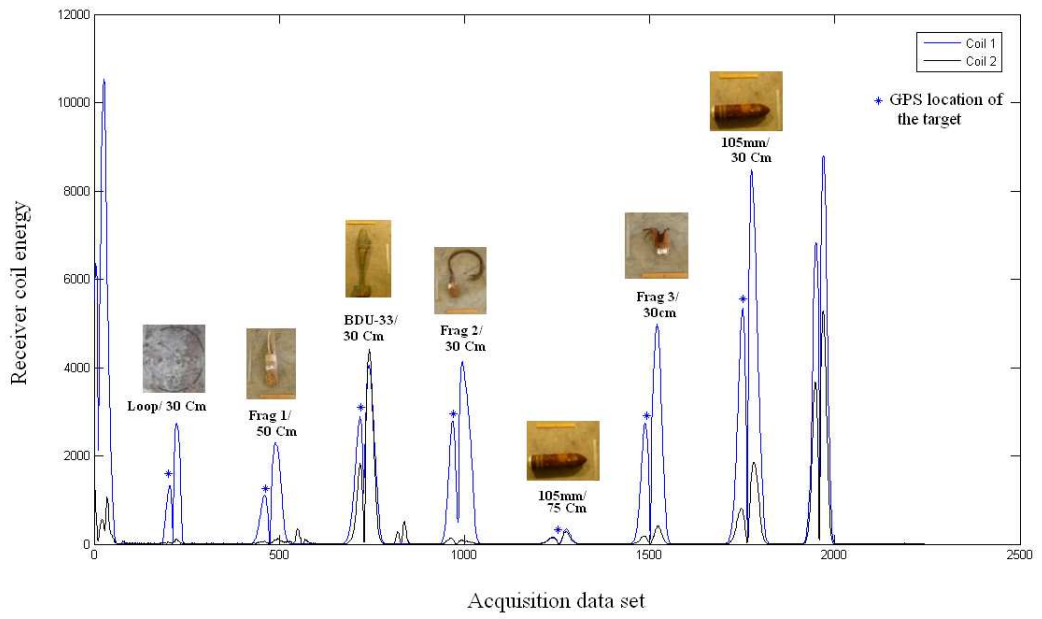


Figure D.7: 2Coil array response, run1 lane1 west to east.

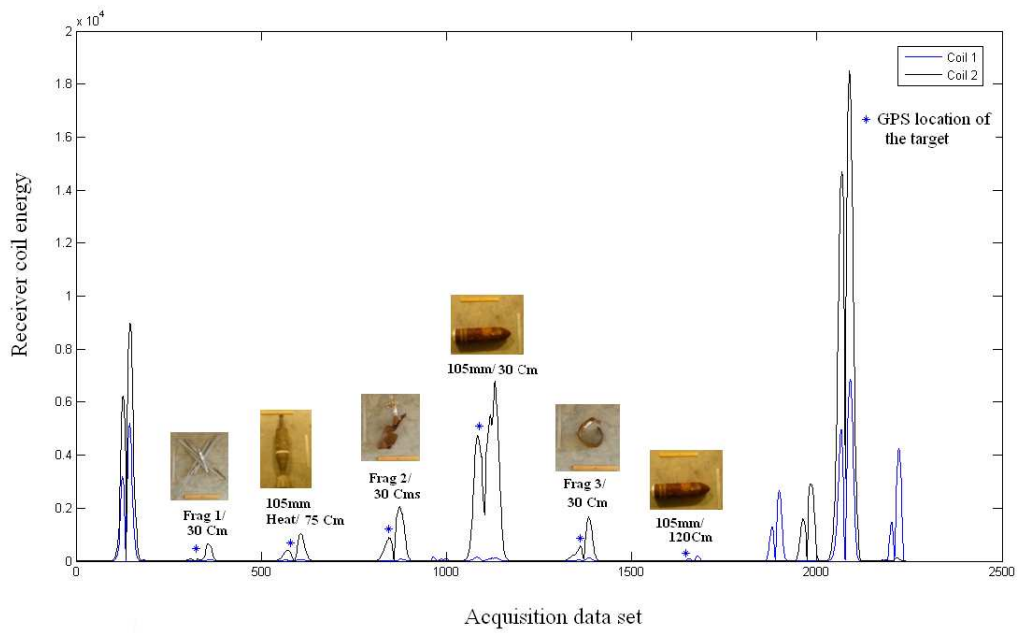


Figure D.8: 2Coil array response, run1 lane2 east to west.

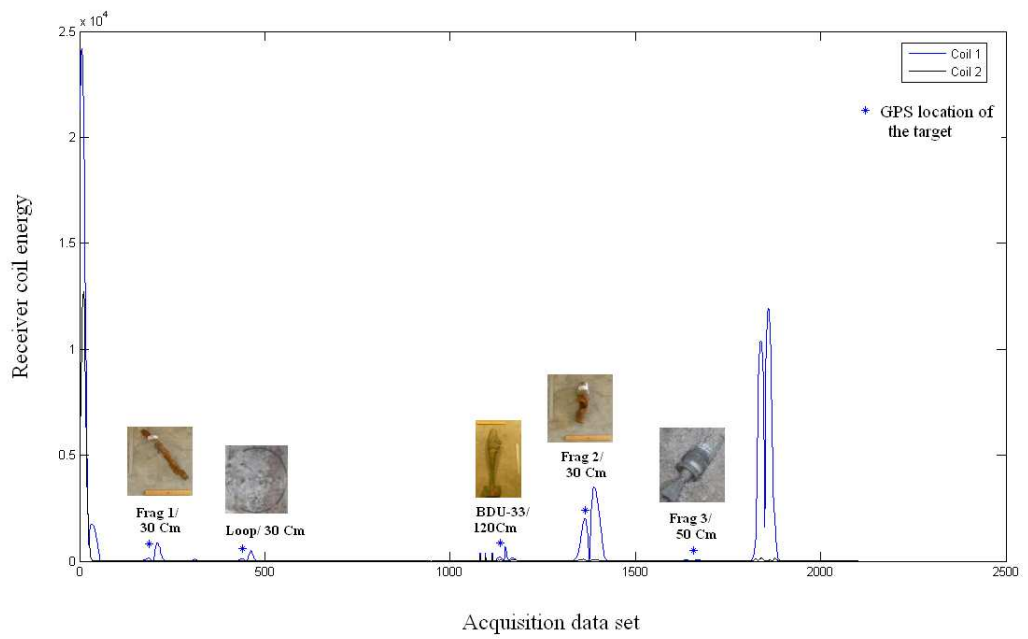


Figure D.9: 2Coil array response, run1 lane3 west to east.

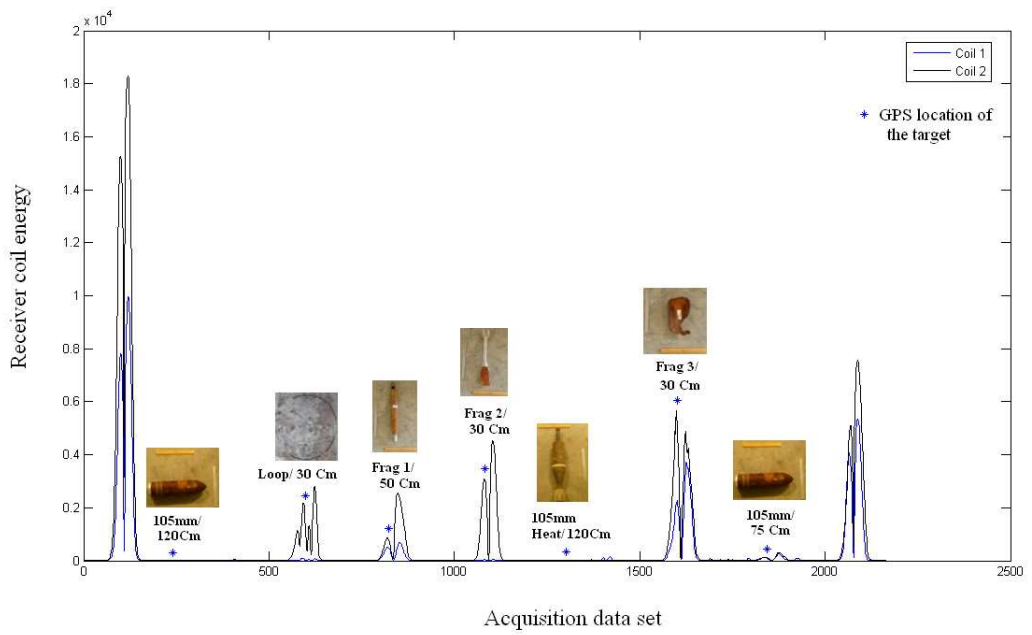


Figure D.10: 2Coil array response, run1 lane4 east to west.

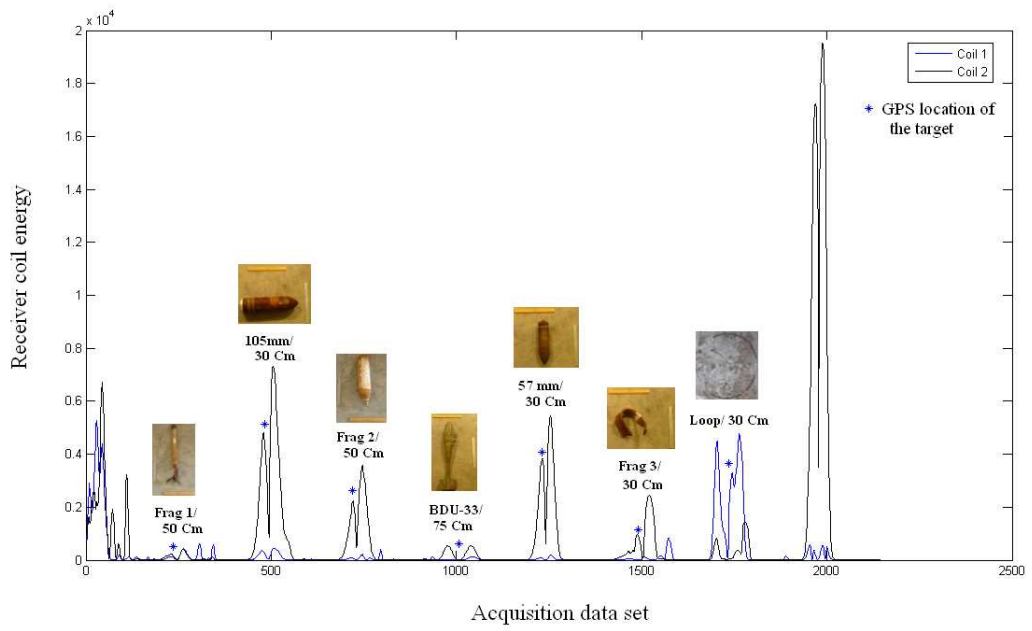


Figure D.11: 2Coil array response, run1 lane5 west to east.

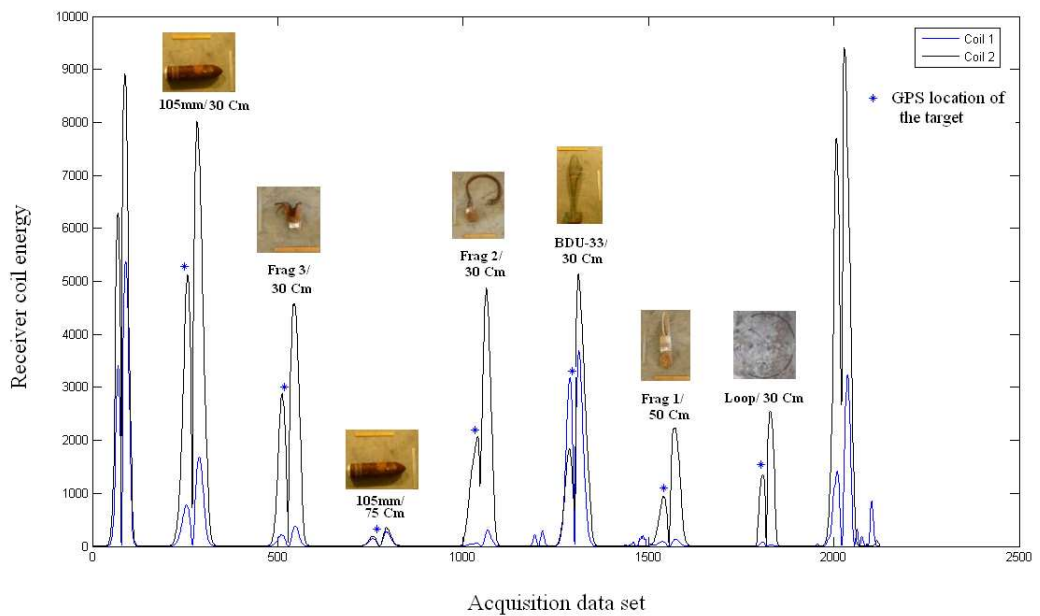


Figure D.12: 2Coil array response, run1 lane1 east to west.

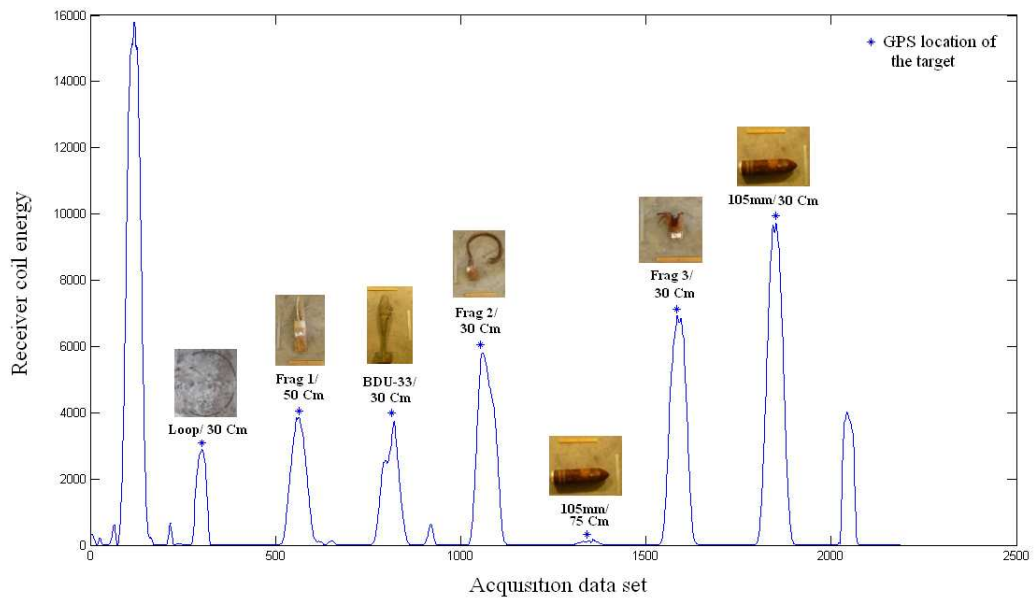


Figure D.13: 1Coil response, run1 lane1 west to east.

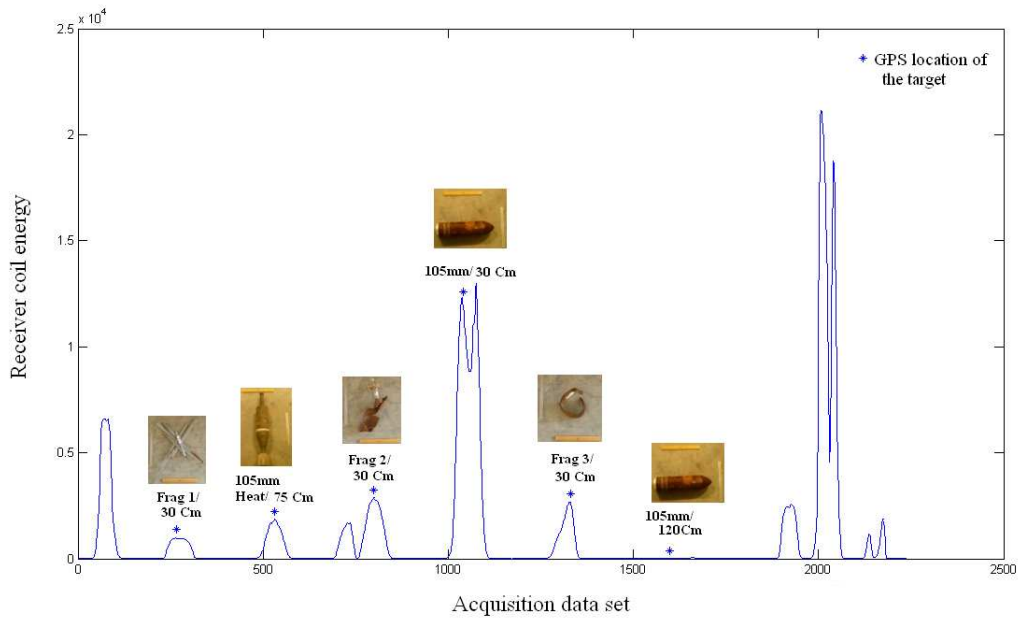


Figure D.14: 1Coil response, run1 lane2 east to west.

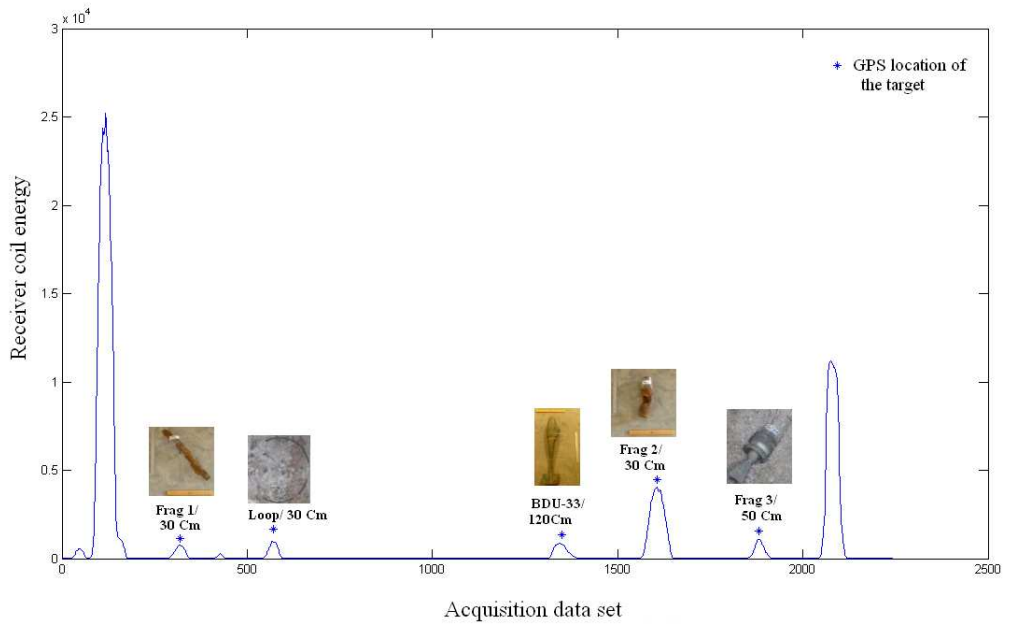


Figure D.15: 1Coil response, run1 lane3 west to east.

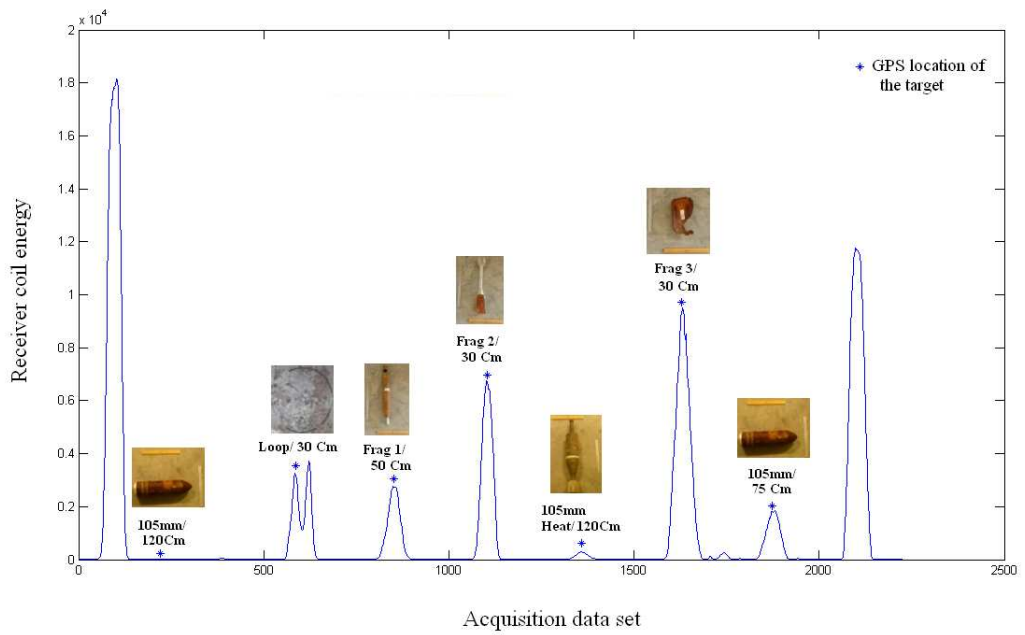


Figure D.16: 1Coil response, run1 lane4 east to west.

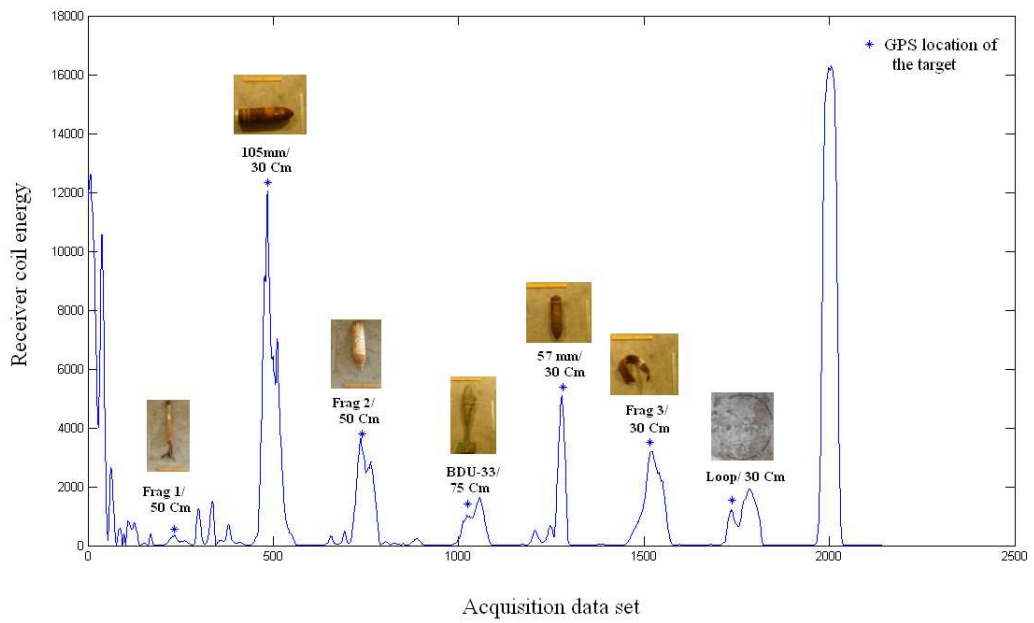


Figure D.17: 1Coil response, run1 lane5 west to east.

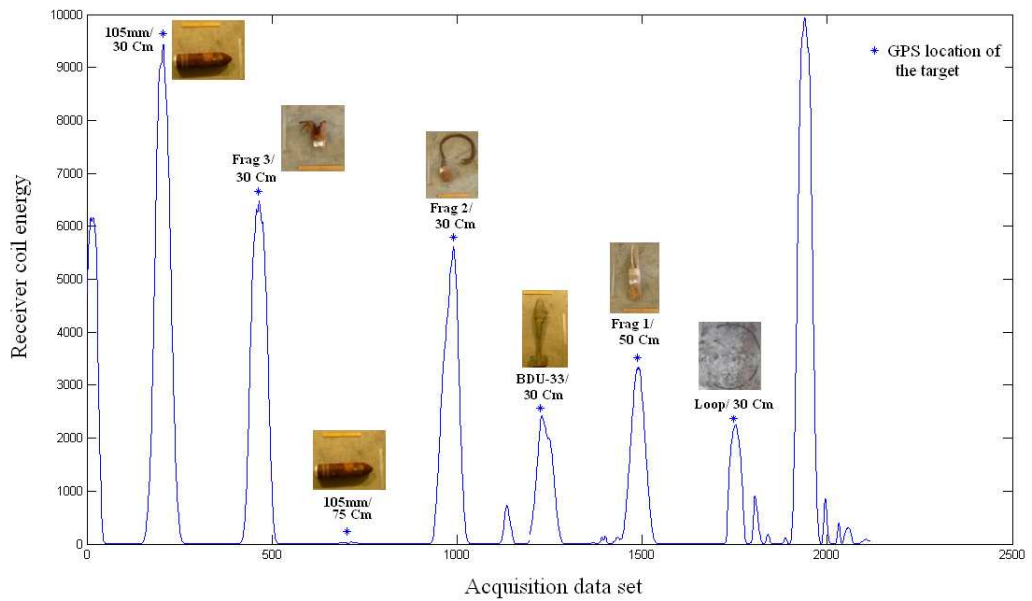


Figure D.18: 1Coil response, run1 lane1 east to west.